ISTANBUL TECHNICAL UNIVERSITY ★ GRADUATE SCHOOL

FRACTURE MECHANICS ON CRITICAL ROTOR COMPONENT IN TURBOJET ENGINE

M.Sc. THESIS

Görkem TÜREN

Department of Aeronautical and Astronautical Engineering

Aeronautical and Astronautical Engineering Programme

AUGUST 2024

ISTANBUL TECHNICAL UNIVERSITY ★ GRADUATE SCHOOL

FRACTURE MECHANICS ON CRITICAL ROTOR COMPONENT IN TURBOJET ENGINE

M.Sc. THESIS

Görkem TÜREN
(511201128)

Department of Aeronautical and Astronautical Engineering

Aeronautical and Astronautical Engineering Programme

Thesis Advisor: Prof. Dr. Halit Süleyman TÜRKMEN

AUGUST 2024

İSTANBUL TEKNİK ÜNİVERSİTESİ ★ LİSANSÜSTÜ EĞİTİM ENSTİTÜSÜ

BİR TURBOJET MOTORUNDA BULUNAN KRİTİK ROTOR KOMPONENTİNDE KIRILMA MEKANİĞİ

YÜKSEK LİSANS TEZİ

Görkem TÜREN
(511201128)

Uçak ve Uzay Mühendisliği Anabilim Dalı

Uçak ve Uzay Mühendisliği Programı

Tez Danışmanı: Prof. Dr. Halit Süleyman TÜRKMEN

AĞUSTOS 2024

Görkem TÜREN, a M.Sc. student of ITU Graduate School Student ID 511201128 successfully defended the thesis entitled "FRACTURE MECHANICS ON CRITICAL ROTOR COMPONENT IN TURBOJET ENGINE", which he prepared after fulfilling the requirements specified in the associated legislations, before the jury whose signatures are below.

Thesis Advisor:	**Prof. Dr. Halit Süleyman TÜRKMEN** Istanbul Technical University	....
Jury Members:	**Prof. Dr. Vedat Ziya DOĞAN** Istanbul Technical University	....
	Dr.Kadir GÜNAYDIN GE Aerospace	....

Date of Submission : 27 July 2024
Date of Defense : 23 August 2024

For my family and whom beside me,

FOREWORD

I would like to extend my deepest gratitude to Prof. Dr. Halit Süleyman TÜRKMEN for his invaluable mentorship, insightful feedback, and commitment to fostering a stimulating academic atmosphere. His expertise, encouragement, and unwavering commitment to my intellectual growth have been instrumental in shaping the trajectory of my research and enhancing the quality of my master's thesis.

In addition to my academic mentor, I am profoundly grateful to my life partner, Kübra, whose unwavering support and understanding have been a source of strength during the challenging phases of my academic journey. Her encouragement and patience have been indispensable, providing me with the emotional fortitude needed to navigate the demands of my studies and thesis completion.

Moreover, I extend my thanks to my colleagues at work who have been instrumental in creating a collaborative and enriching professional environment. Their willingness to share knowledge, engage in meaningful discussions, and provide assistance has greatly contributed to the depth and breadth of my research. Their support has been invaluable, fostering an environment where ideas flourish and where I could benefit from their diverse expertise. I am truly appreciative of their collective efforts, which have significantly enriched the quality of my work and contributed to the successful completion of this thesis.

July 2024

Görkem Türen
Engineer

TABLE OF CONTENTS

Page

FOREWORD .... **ix**
TABLE OF CONTENTS .... **xi**
ABBREVIATIONS .... **xiii**
LIST OF SYMBOLS .... **xv**
LIST OF TABLES .... **xvii**
LIST OF FIGURES .... **xix**
SUMMARY .... **xxi**
ÖZET .... **xxiii**
1. INTRODUCTION **27**
1.1 Purpose of Thesis 28
1.2 Literature Overview 28
1.3 Outline of Thesis 30
2. THEORETICAL BACKGROUND **31**
2.1 Linear Elastic Fracture Mechanics (LEFM) 31
2.1.1 Stress concentration factor 31
2.1.2 Griffith’s energy criterion 32
2.1.3.1 Loading modes of fracture 33
2.1.3.2 Geometric correction factor 35
2.2 Elasto-Plastic Fracture Mechanics 35
2.2.1 J-Integral 36
2.3 Paris-Erdogan Crack Propagation Law 36
2.4 Machine Learning and its Algorithms 38
3. NUMERICAL AND ANALYTICAL METHODS **41**
3.1 First Study: Compact Tension Test Specimen (CTT) 41
3.1.1 Compact Tension Test specimen geometry 42
3.1.2 Analytical method 43
3.1.3 Numerical analysis 44
3.1.3.1 Geometry 45
3.1.3.2 Material 45
3.1.3.3 Modelling 49
3.2 Second Study: LEFM on a Turbine Blade of Turbojet Engine 53
3.2.1 The turbine geometry 54
3.2.2 Material 55
3.2.3 Numerical analysis 56
3.2.3.1 Elastic structural analysis 56
3.2.3.2 LEFM on turbine geometry 60
3.3 The Third Study: Machine Learning Algorithm for prediction of LEFM Parameters 63
3.3.1 The machine learning algorithm 64
4. RESULTS AND COMPARISON **67**

4.1 First Study: Compact Tension Test Specimen (CTT) Results 67
4.1.1 The analytical results... 67
4.1.2 Numerical solutions.. 68
4.1.2.1 Stress intensity factors.. 70
4.1.2.2 J integral results.. 73
4.1.2.3 Result comparison of stress intensity factor........................ 76
4.1.2.4 Result comparison of elastic j integral 76
4.2 Second Study: LEFM on a Turbine Blade 76
4.3 The Results of the Machine Learning Model 80
5. CONCLUSIONS AND RECOMMENDATIONS 83
REFERENCES 85
CURRICULUM VITAE 87

ABBREVIATIONS

ASTM	**:** American Society for Testing and Materials
BEM	**:** Boundary Element Method
CTT	**:** Compact Tension Test Specimen
EPFM	**:** Elasto-Plastic Fracture Mechanics
FEM	**:** Finite Element Method
LEFM	**:** Linear Elastic Fracture Mechanics
SCF	**:** Stress Concentration Factor
SIF	**:** Stress Intensity Factor
XFEM	**:** Extended Finite Element Method

LIST OF SYMBOLS

a	:Crack length
da	:Crack increment
E	:Young’s modulus
E_t	:Tangential modulus
G	:Elastic energy release rate
G_c	:Critical elastic energy release rate
J	:J-integral
K	:Stress intensity factor
K_c	:Critical value of the stress intensity factor
K_I	:Stress intensity factor for Mode I
K_{Ic}	:Fracture toughness
K_{II}	:Stress intensity factor for Mode II
K_{III}	:Stress intensity factor for Mode III
P	:Loading
w	:Strain energy density
x, y	:Cartesian coordinates
ν	:Poisson’s ratio
μ	:Shear modulus

LIST OF TABLES

Table 3.1 : Material properties of Ti-6Al-4V.. 46
Table 3.2 : True plastic strain stress values of titanium alloy.................................... 49
Table 3.3 : Generally used gas turbine materials. 55
Table 3.4 : Ti-6242 material properties.. 56
Table 3.5 : Paris Law parameters of Ti-6242... 56
Table 4.1 : Stress intensity factors for all analyses. 76
Table 4.2 : Elastic J-Integral results for all analyses.. 76

LIST OF FIGURES

Page
Figure 2.1 : General representation of the crack tip. 31
Figure 2.2 : Loading mode types of a crack. 33
Figure 2.3 : Tensor component representation on the crack tip. 34
Figure 2.4 : Fatigue crack growth rate. 37
Figure 2.5 : Machine learning algorithms. 38
Figure 3.1 : Compact tension test specimen. 42
Figure 3.2 : Typical CTT parameters. 43
Figure 3.3 : Typical mesh flow in ANSYS. 44
Figure 3.4 : 2D and 3D representation of CTT. 45
Figure 3.5 : Symmetric 2D and 3D geometries of CTT. 45
Figure 3.6 : Engineering stress-strain curve of Ti-6Al-4V. 47
Figure 3.7 : Engineering stress strain vs true stress strain curve. 48
Figure 3.8 : The geometric details of 2D model. 50
Figure 3.9 : Symmetry boundary condition. 50
Figure 3.10 : The mesh refinement at the crack tip. 51
Figure 3.11 : Final mesh distribution of 2D geometry. 51
Figure 3.12 : Pre-meshed crack feature. 51
Figure 3.13 : Boundary and loading conditions. 52
Figure 3.14 : Symmetry region of 3D model. 52
Figure 3.15 : Final mesh representation of 3D geometry. 53
Figure 3.16 : Boundary condition and loading conditions of 3D model. 53
Figure 3.17 : General Electric CF6 turbine blade. 54
Figure 3.18 : 3D blade geometry drawn in SOLIDWORKS. 55
Figure 3.19 : Turbine geometry. 57
Figure 3.20 : Bodies with sweep mesh control. 58
Figure 3.21 : Mesh distribution of turbine blade. 58
Figure 3.22 : Boundary condition of the turbine blade. 59
Figure 3.23 : Total deformation and radial deformation of the turbine blade. 59
Figure 3.24 : Equivalent stress distribution of the turbine blade. 60
Figure 3.25 : Basic turbine blade geometry. 61
Figure 3.26 : Crack definition of the turbine blade. 61
Figure 3.27 : Crack tip mesh refinement. 62
Figure 3.28 : Boundary condition and loading conditions of the turbine blade. 62
Figure 3.29 : Geomerty dimensions of 2D symmetric model. 63
Figure 3.30 : Parametric equation of 2D symmetric model 64
Figure 3.31 : Parametric input and output values in ANSYS Mechanical. 64
Figure 3.32 : Stress intensity factor curve. 65
Figure 3.33 : Logarithmic stress intensity factor values. 66
Figure 3.34 : Linear regression command line. 66
Figure 3.35 : Prediction function of the machine learning code. 66
Figure 4.1 : 2D elastic analysis- total deformation. 69

Figure 4.2 : 3D elastic analysis- total deformation. 69
Figure 4.3 : 2D plastic analysis- total deformation. 69
Figure 4.4 : 3D plastic analysis- total deformation. 70
Figure 4.5 : The maximum stress intensity factor of 2d elastic model. 70
Figure 4.6 : The maximum stress intensity factor of 2d plastic model. 71
Figure 4.7 : Stress intensity factor distribution of 3d elastic model. 71
Figure 4.8 : K_1 distribution along specimen thickness. 72
Figure 4.9 : Stress intensity factor distribution of 3d plastic model. 72
Figure 4.10 : K_1 distribution along specimen thickness. 73
Figure 4.11 : Elastic J-Integral results of 2D elastic model. 73
Figure 4.12 : Total J-Integral results of 2D plastic model. 74
Figure 4.13 : Elastic J-Integral results of 3D elastic model. 74
Figure 4.14 : Elastic J-Integral distribution of 3D elastic model. 74
Figure 4.15 : Total J-Integral results of 3D plastic model. 75
Figure 4.16 : Total J-Integral distribution of 3D plastic model. 75
Figure 4.17 : Crack extension vs analysis time. 77
Figure 4.18 : The crack extension versus total number of cycles. 77
Figure 4.19 : Crack propagation of the turbine blade. 78
Figure 4.20 : Total deformation versus analysis time of the turbine blade analysis. . 78
Figure 4.21 : The maximum stress intensity factor at the end of the analysis. 79
Figure 4.22 : Stress intensity factor contours. 79
Figure 4.23 : Predicted values vs finite element results. 80
Figure 4.24 : Residual plot of the machine learning model. 81

FRACTURE MECHANICS ON CRITICAL ROTOR COMPONENT IN TURBOJET ENGINE

SUMMARY

The occurrence of crack initiation in a rotor component within turbo-engines poses a substantial threat, given the potential for severe engine failure due to the high-speed rotation and harsh operational conditions. To enhance engine durability and safety, a comprehensive understanding of fracture mechanics is necessary.

The thesis incorporates a triple-pronged approach to calculating crack fatigue life and related fracture mechanics parameters such as stress intensity factor and J-Integral. In the first approach, a compact tension test (CTT) specimen was investigated in terms of both Linear Elastic Fracture Mechanics (LEFM) and Elastic Plastic Fracture Mechanics (EPFM) by using 2D and 3D analysis methods. These analysis results were compared with empirical formulations available in the literature. The main goal of first study is creating a baseline for third study.

In the second approach, a turbine geometry with firtree structure was drawn by utilizing NACA airfoils as a baseline. After geometry adaptation, Finite Element Method (FEM) is leveraged using ANSYS In the analysis model, Linear Elastic Fracture Mechanics was deployed with linear material model. To ascertain stress values in proximity to the crack tip, a static structural analysis with elastic material properties is conducted, considering rotational velocity loading.

In the third approach, a parametric study was conducted by using the same compact tension test specimen in first approach by changing geometric parameters such as plate thickness, specimen width, load values using ANSYS Mechanical. After having 250 different solution combination of the analysis, these parameters were exported as a data file in order to use in a machine learning model. A linear regression machine learning model was deployed by using sklearn's machine learning libraries.

In the final stages of the study, the results gathered from both the ANSYS simulation and the numerical method are rigorously compared, providing a nuanced understanding of the agreement and discrepancies between these analytical approaches. This comparative analysis not only validates the robustness of the chosen methodologies but also contributes to a deeper comprehension of the factors influencing crack propagation in turbine blades within the specified operational contexts.

BİR TURBOJET MOTORUNDA BULUNAN KRİTİK ROTOR KOMPONENTİNDE ÇATLAK MEKANİĞİ

ÖZET

Rotor bileşenlerinde çatlak başlangıcının meydana gelmesi, turbo motorlar için ciddi bir tehdit oluşturmaktadır; çünkü yüksek hızda dönen ve zorlu çalışma koşullarına maruz kalan bu motorlarda çatlak, ciddi motor arızalarına yol açabilir. Turbo motorlar, havacılık, enerji üretimi ve endüstriyel uygulamalar gibi birçok alanda kritik bir rol oynar ve bu tür motorların güvenilirliği, performansı ve uzun ömürlülüğü büyük ölçüde, rotor bileşenlerinde meydana gelen yorulma ve kırılma süreçlerinin anlaşılmasına bağlıdır. Yüksek devir hızlarında çalışan turbo motorlarda, çatlakların erken tespiti ve ilerlemesinin tahmini, motorların genel güvenliği ve verimliliği açısından hayati öneme sahiptir. Özellikle bu tür motorların maruz kaldığı termal ve mekanik yükler, rotor bileşenlerinde yüksek gerilme konsantrasyonlarına neden olabilir ve bu da çatlakların büyümesine ve olası ani arızalara yol açabilir. Bu nedenle, bu motorların performansını ve güvenliğini sağlamak için kırılma mekaniği prensiplerinin derinlemesine anlaşılması ve bu prensiplerin mühendislik uygulamalarında etkin bir şekilde kullanılması kritik bir gerekliliktir.

Kırılma mekaniği, çatlakların oluşumunu, ilerlemesini ve son kırılmayı tahmin etmede önemli bir bilimsel alan olup, mühendislerin motor tasarımı sırasında güvenilirlik ve dayanıklılığı optimize etmelerini sağlar. Çatlak ilerlemesi ve yorulma ömrü tahminleri, rotor bileşenlerinin malzeme seçimi, geometrik yapılandırmaları ve operasyonel yükleme koşulları ile doğrudan ilişkilidir. Dolayısıyla, kırılma mekaniği yaklaşımlarını kullanarak turbo motor bileşenlerinde güvenliği artırmak için hem teorik hem de pratik bilgiler bir araya getirilmelidir.

Lineer Elastik Kırılma Mekaniği (LEKM) **ve** Elastik Plastik Kırılma Mekaniği (EPKM)**,** çatlakların malzemeler üzerindeki etkilerini ve ilerlemesini analiz etmek için kullanılan iki temel kırılma mekaniği yaklaşımıdır ve turbo motor bileşenlerinde çatlak yorulma ömrü analizleri için kritik öneme sahiptir. Lineer Elastik Kırılma Mekaniği (LEKM), malzemenin elastik davranışını temel alarak çatlak uçlarında oluşan gerilme yoğunluğunu ve deformasyonları inceleyen bir yöntemdir. Bu yaklaşım, malzemenin doğrusal elastik davranış gösterdiği durumlarda ve çatlak boyutunun, malzeme elastikiyetine kıyasla küçük olduğu senaryolarda uygulanır. LEFM, özellikle çatlak ucu etrafındaki gerilme yoğunluk faktörünü (K) kullanarak çatlak ilerlemesini öngörür ve bu yöntemle hesaplamalar, turbo motor bileşenlerinde, yüksek hız ve zorlu şartlar altında oluşabilecek çatlak başlangıcı ve ilerlemesinin tahmin edilmesine olanak tanır.

Öte yandan, Elastik plastik Kırılma Mekaniği (EPKM), malzemenin doğrusal elastik sınırlarını aşarak plastik deformasyon göstermeye başladığı durumları analiz etmek için kullanılır. EPKM, özellikle çatlak ucu bölgesinde plastik bölgenin önemli hale geldiği ve malzemenin doğrusal elastik sınırın ötesine geçtiği senaryolarda uygulanır. Bu yaklaşım, J-Integrali ve çatlak ucu açıklık deplasmanı (CUAD) gibi parametreleri kullanarak çatlak ilerlemesinin daha karmaşık bir şekilde modellenmesine olanak

tanır. EPFM, özellikle yüksek gerilmeli bölgelerde veya plastik deformasyonun belirgin olduğu malzemelerde çatlak ilerlemesi tahminleri için kullanılır ve turbo motor bileşenlerinin zorlu çalışma koşullarına dayanıklılığını değerlendirmede önemli bir araçtır. Bu iki kırılma mekaniği yaklaşımı, turbo motor bileşenlerinin tasarımı ve analizinde kritik rol oynar; zira her iki yöntem de çatlak oluşumu ve ilerlemesi üzerinde farklı perspektifler sunarak, bileşenlerin güvenilirliğini ve uzun ömürlülüğünü artırmaya yönelik stratejilerin geliştirilmesine katkıda bulunur.

Bu tez, çatlak yorulma ömrünün hesaplanması ve gerilme yoğunluğu faktörü (K) ve J-Integrali gibi ilgili kırılma mekaniği parametrelerinin belirlenmesi için üç aşamalı bir yaklaşımı içermektedir.

İlk yaklaşımda, kompakt gerilim testi numunesi, hem Lineer Elastik Kırılma Mekaniği (LEFM) hem de Elastik Plastik Kırılma Mekaniği (EPFM) perspektiflerinden incelenmiştir. Bu numune, metalik malzemelerin kırılma tokluğu açısından bir referans noktası oluşturmak amacıyla, çeşitli testlerin gerçekleştirildiği test laboratuvarlarında yaygın olarak kullanılmaktadır. Bu testler, malzemenin çatlakların yükleme yönüne dik olarak ilerlemesi durumunda kırılmaya karşı gösterdiği direnci değerlendirmeye yönelik olarak tasarlanmıştır. Söz konusu numune, doğal bir çatlak oluşumunu simüle edecek şekilde, işlenmiş bir çentiğe ve yorulma çatlağına sahip küçük, dikdörtgen bir yapıdadır. Test sürecinde, numune kontrollü bir şekilde yük altına alınarak kırılma noktasına kadar zorlanır ve bu süreçte kritik gerilme yoğunluk faktörü (K) değeri hesaplanır. Elde edilen bu kritik değer, özellikle gevrek kırılma riskinin bulunduğu yapısal uygulamalarda malzemenin davranışını ve güvenilirliğini anlamak açısından son derece önemlidir. Bu tür değerlendirmeler, mühendislik yapılarında olası arızaların önlenmesine yönelik tasarım ve malzeme seçim süreçlerine önemli katkılar sağlar. Bu çalışmada ise bahsedilen incemeler, iki boyutlu (2D) ve üç boyutlu (3D) analiz yöntemleri kullanılarak gerçekleştirilmiştir. Buradaki analiz modelindeki çıktılar, lineer elastik kırılma mekaniğinde sıklıkla kullanılan gerilme yoğunluğu faktörü ve elastik plastik kırılma mekaniğinde sıklıkla kullanılan hem elastik hem de plastik J Integral değerleridir. Buradaki modelde ana malzeme olarak Titanyum 6-4 seçilmiştir. Malzeme bilgileri ANSYS Granta Malzeme Modülünden direkt olarak alınmıştır. Fakat, buradaki malzeme modelinde sadece elastik bilgiler vardır. Plastik malzeme modeli oluşturmak için Ramberg- Osgood denklemleri kullanılarak önce mühendislik gerilme ve gerinim değerleri elde edilmiştir. Plastik malzeme modelinin elde edilmesi için Neuber formülasyonları da kullanılıp en son gerçek gerilme ve gerinim değerleri ANSYS malzeme modeline eklenmiştir. Gerçek hayattaki test senaryosuna uyumlu olacak şekilde yükleme koşulları uygulanmıştır. Elde edilen analiz sonuçları, Amerikan Test ve Malzeme Derneği (ASTM) tarafından sunulan empirik formüllerle karşılaştırılmıştır. Bu çalışmanın temel amacı, kırılma mekaniği analizlerinde kullanılan yöntemlerin doğruluğunu değerlendirmek ve daha sonraki çalışmalar için bir temel oluşturmaktır. Buradaki ilk çalışmanın amacı, üçüncü yaklaşımda kullanılacak makine öğrenmesi modeli için bir referans noktası ve doğrulama temeli oluşturmaktır.

İkinci yaklaşımda, bir türbin geometrisi, firtree yapısına sahip olacak şekilde tasarlanmış ve NACA hava kanat profilleri temel alınarak modellenmiştir. Geometri oluşturulmasının ardından, Sonlu Elemanlar Yöntemi (FEM) kullanılarak ANSYS Separating Morphing and Adaptive Remeshing Technology (SMART) modülü ile ayrıntılı bir analiz gerçekleştirilmiştir. Bu analiz modelinde, lineer malzeme modeli ile Lineer Elastik Kırılma Mekaniği kullanılmıştır. Malzeme modeli olarak literatürde çokça kullanılan ve üzerine çalışmalar yapılmış Titanyum 6242 seçilmiştir. Bu malzeme modeline ek olarak, geometri üzerinde bulunan çatlağın ömrünün hesaplanması için Paris Erdoğan Yasası katsayısı da dahil edilmiştir. Çatlak ucuna yakın bölgelerdeki gerilme değerlerini belirlemek amacıyla, dönme hızına bağlı yüklemeler dikkate alınarak elastik malzeme özellikleri kullanılarak statik bir yapısal analiz yapılmıştır. Bu yaklaşım, rotor bileşenlerindeki gerilme yoğunluğunun hangi bölgelerde olacağına ve bu değerlerin hassas bir şekilde hesaplanmasına ve çatlak başlangıcının tahmin edilmesine odaklanmıştır. Analizin sonucunda çatlağın belirli yükleme koşulunda ve Paris-Erdoğan Yasası kapsamında çatlağın ilerleme hızını, çatlağın parça üzerinde ömür açısından etkisini açık bir şekilde ortaya koymuştur.

Üçüncü yaklaşımda, ilk çalışmada kullanılan kompakt gerilim testi numunesi üzerinde çeşitli geometrik parametreler (örneğin, plaka kalınlığı, numune genişliği, yük değerleri) değiştirilerek parametrik bir çalışma yürütülmüştür. Bu çalışmadaki öncelikli çıktılar gerilme yoğunluğu faktörü (K) ve Elastik J Integral değerlerini hesaplamaktır. ANSYS Mechanical kullanılarak yapılan bu analizlerde, toplamda 250 farklı çözüm kombinasyonu elde edilmiştir. Bu analizlerin sonuçları bir veri dosyası olarak dışa aktarılmış ve bir makine öğrenimi modelinde kullanılmak üzere hazırlanmıştır. sklearn kütüphaneleri kullanılarak lineer regresyon tabanlı bir makine öğrenimi modeli oluşturulmuştur. Bu model, kırılma mekaniği parametrelerinin ve çatlak ilerlemesinin öngörülmesine yönelik tahminler yapabilmektedir.

Çalışmanın son aşamalarında hem ANSYS simülasyonu hem de geliştirilen sayısal yöntemlerden elde edilen sonuçlar titizlikle karşılaştırılmıştır. Bu karşılaştırmalı analiz, analitik yaklaşımlar arasındaki uyum ve farklılıkların kapsamlı bir şekilde anlaşılmasını sağlamış ve yöntemlerin güvenilirliğini değerlendirmeye yönelik kritik bir bakış açısı sunmuştur. Analiz sonuçlarının karşılaştırılması, seçilen metodolojilerin sağlamlığını ve geçerliliğini doğrulamakla kalmamış, aynı zamanda türbin kanatları gibi rotor bileşenlerinde belirli çalışma koşulları altında çatlak ilerlemesini etkileyen faktörlerin daha derin bir şekilde anlaşılmasına katkıda bulunmuştur.

Bu geniş kapsamlı araştırma, turbo motor bileşenlerinde çatlak oluşumu ve ilerlemesi konusundaki bilgi birikimine önemli katkılarda bulunmaktadır. Çalışma, kırılma mekaniği ve yorulma ömrü analizlerinde yenilikçi yaklaşımlar, sayısal yöntemler ve ileri düzey simülasyon teknikleri sunarak bu alandaki mühendislik problemlerinin çözümüne yönelik önemli bir kaynak oluşturmaktadır. Bu bağlamda, elde edilen bulgular ve önerilen metodolojiler, rotor bileşenlerinin güvenilirliğini artırmak ve operasyonel güvenliği sağlamak için değerli bilgiler sunmaktadır. İleride bu çalışma kullanılarak, özellikle makine öğrenmesi konusunda daha gelişmiş düzeylerde çalışmalar yapılabilir.

1. INTRODUCTION

In today's world, people being try to achieve a standard in manufacturing about usefulness and sustainability. Therefore, they need to complete some testing process to verify whether the product satisfies the expectation. However, it is not always possible to test a product after it is manufactured. In this situation, numerical and analytical approaches become a significant asset in terms of validation.

Due to the nature of the aviation sector, aircraft engines require high power and structural integrity to satisfy demands securely. Therefore, it is a must to complete these validation processes carefully.

Throughout their time in service, aircraft engines are subjected to a variety of extremely demanding operating circumstances, including high temperatures, constant pressure, fast rotating speeds, and corrosive environments. These engines run at a variety of temperatures, from extremely cold temperatures experienced during high-altitude flights to intense heat produced by the combustion chambers. Because aircraft engines run in harsh environments and their parts are subjected to cyclic loads, fatigue and fracture mechanics are essential to maintaining the dependability and safety of these engines. Engine materials experience considerable fatigue as a result of the cyclical loads brought on by the repeated takeoff, flying, and landing operations. This might eventually result in structural breakdowns. These recurrent stress cycles can cause fatigue cracks to form and spread, which poses a serious risk to the structural integrity of the engine. To forecast, identify, and mitigate such cracks, one must have a solid understanding of fatigue and fracture mechanics.

Fracture Mechanics is an area of study within the fields of materials science and mechanical engineering, focused on investigating the response of materials to external forces that lead to the initiation, propagation, and ultimate failure of cracks. Its objective is to gain insight into the fundamental mechanisms and properties of cracks in materials, thereby enhancing our understanding of how materials withstand stress, load, and environmental factors, ultimately influencing their structural reliability.

1.1 Purpose of Thesis

The study of thesis focuses on three different studies in terms of fracture mechanics applications. The main objective of this thesis is a creating a perspective and a starting point to the fracture mechanics in terms of importance in the aviation history. Moreover, a machine learning model is implemented to use in feature studies.

1.2 Literature Overview

Fracture mechanics interest on the behavior and failure of structures under stress or load has increased in recent years. This interest has led to numerous studies and advancements in understanding the mechanisms and prediction of fractures in various materials.

First disaster seen as the birth of fracture mechanics may be a tanker named as SS Schenectady which used in World War 2 by United States. In 1943, The SS Schenectady was conducting launch preparations while still on the slipway when it abruptly had a structural breakdown that split it in half. [1] The primary cause of the breakdown was brittle fracture brought on by a temperature shift. This catastrophe has become a landmark in the field of fracture mechanics.

In the history, first breakthrough about fracture mechanics studies starts with work of Griffith (1880-1963). The contributions of Griffith marked the genuine birth of fracture mechanics in 1920. Inspired by the perplexing mismatch between glass's actual and theoretical tensile strength, he put out a ground-breaking theory: cracks in the structures function as stress concentrators, decreasing the material's effective strength and opening the door to catastrophic collapse [2].

In following years, Irwin suggested a phenomenon called as Stress Intensity Factor (SIF) in his crack studies about plates 1957. This parameter indicates that the stress intensity factor stated as K, which is a critical parameter in linear elastic fracture mechanics (LEFM), may be used to define the size and form of the plastic zone surrounding the crack tip. [3]

Nonetheless, all of these studies did not contain any information about crack propagation and fatigue life. In 1961, Paris et al. found a new way to define crack propagation and its life by defining new equation called as Paris-Erdogan Law [4].

According to the equation, the rate of fracture development is exactly correlated to the range of the stress intensity factor multiplied by another material constant.

Prior to the late 1960s, understanding crack behaviors in fracture mechanics presented significant challenges due to the widespread use of linear approaches. The complexities of non-linearities in material properties, loading conditions, and geometric configurations presented formidable challenges. It became clear that traditional methodologies failed to adequately capture the complexities of plastic materials, limiting the accuracy of fracture toughness assessments. In 1968, Rice developed the J-integral, which provides a path-independent metric of fracture toughness that is particularly useful for plastic materials.[5]

In early 2000's, Finite Element Method (FEM) and extended-Finite Element Method (X-FEM) its software were started to getting attentions from all around the world about fracture mechanics. In 2003, Novati and Frangi proposed a different approach technique by coupling Boundary Element Method (BEM) and Finite Element Method (FEM) for near-crack region. [6] In 2012, Tran and Geniaut released a study about fracture mechanic calculations of an axisymmetric model of cylindrical tube with a crack by using X-FEM Method. In this study, different welding conditions were investigated and compared with available literature data. [7] In 2016, Mamandi and Rajabi applied fracture mechanics and fatigue crack growth life on a turbine blade by using Finite Element Method. The results were compared with analytical calculations.[8]

Over the last ten years, the machine learning industry's latest advancements have prompted research on probabilistic techniques in fracture mechanics. In 2017, Krejsa et al proposed a probabilistic prediction of the fatigue damage by using linear elastic fracture mechanics parameters. The paper presents a detailed probabilistic assessment of a steel structural element subject to fatigue load, emphasizing edge and surface cracks using Direct Optimized Probabilistic Calculation (DOPRoC). [9]

1.3 Outline of Thesis

There are three different approaches in this thesis.

In the first study, a compact tension test specimen (CTT) under a tensile loading has been investigated in terms of different geometric and loading parameters. Different parameters were compared with each other such as stress intensity factor, J Integral.

In the second study, the fracture mechanics theory was investigated on a critical component located in a turbojet engine subjected to cyclic loads in terms of Linear Elastic Fracture Mechanics (LEFM) by using a commercial Finite Element Method code. Results were compared for various parameters.

In the final study, a machine learning code was written by obtaining parametric results from the first study of CTT. The main goal was creating a user-friendly environment by training a machine learning model in Sklearn.

In the second part, required theoretical background of Linear Elastic Fracture Mechanics and Elasto-Plastic Fracture Mechanics are presented. The third chapter introduces the main methodology about analytical solutions and numerical solutions. After that, the results are presented and discussed in the fourth chapter.

2. THEORETICAL BACKGROUND

2.1 Linear Elastic Fracture Mechanics (LEFM)

Linear Elastic Fracture Mechanics (LEFM) is a branch of the fracture mechanics for understanding and analyzing the behavior of cracks in the structures which have external loadings. For these formulations, the material should behave as elastic where the Hooke's Law applies. In Linear Elastic Fracture Mechanics, Stress Intensity Factor is the most used parameter in order to describe behavior of the crack. This parameter will be introduced in further section.

In Figure 2.1 the representation of the crack tip is shown. When a crack occurs on the structure, a singularity zone is created by the nature of a crack. In this zone, there are different plastic zones which exceed the yield point of the material. Linear Elastic Fracture Mechanics formulas are valid if the plastic zone at the crack tip is smaller and neglectable when it is compared with elastic singularity zone.[10]

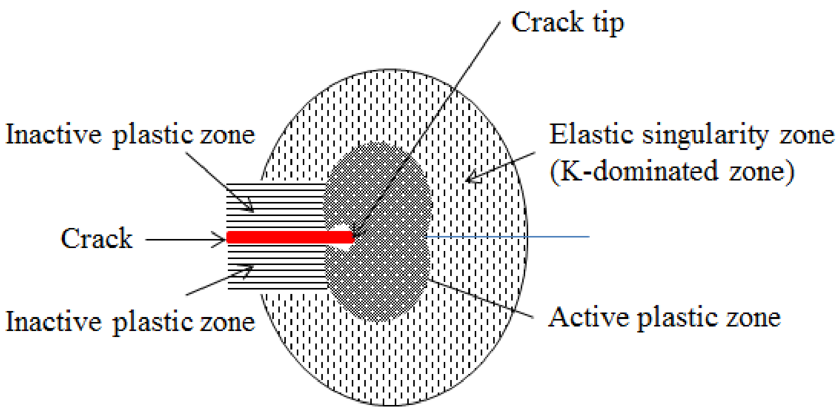

Figure 2.1 : General representation of the crack tip.

2.1.1 Stress concentration factor

The stress concentration factor (k_t) is a dimensionless parameter used in engineering and materials research to quantify how much stress is amplified or concentrated at certain points, such as notches, holes, fractures, or changes in structures. [11] These geometric discontinuities cause stress amplification when the stress value at the peak point is compared with the nominal stress value. This relationship is given as:

$$\sigma_{\text{concentrated}} = k_t . \sigma_{\text{nominal}} \quad (2.1)$$

A k_t value of 1 indicates that there is no stress concentration, but values more than 1 shows that there is stress amplification. This approximation is valid various type of features including notches, fillets, holes.

This parameter is based on the geometry. Therefore, it is hard and sometimes impossible to calculate k_t value for complex geometries such as ones includes sharp edges as in cracks.

2.1.2 Griffith's energy criterion

Griffith's Energy Criterion method is a cornerstone in fracture mechanics era. This methodology shows that a crack will propagate when the rate of decrease in potential energy stored in the material due to crack growth becomes equal to or greater than the rate of increase in surface energy which is required to create new crack surfaces [2]. The Equation 2.2 states the relationship mentioned above:

$$G_c = \frac{\pi \sigma^2 a}{E} \quad (2.2)$$

Where G is elastic energy release rate per unit material thickness, σ is stress value at the crack, a is the half crack length and E is the Young's Modulus of the material used in the geometry.

If the stress is left alone, the equation become:

$$\sigma = \sqrt{\frac{E G_c}{\pi a}} \quad (2.3)$$

This formulation is valid for problem which behaves as plane stress. In order to comply it with plane strain problems, one should change the formulation as below:

$$\sigma = \sqrt{\frac{EG_c}{\pi a(1 - v^2)}} \tag{2.4}$$

Where v is the Poisson's Ratio of the material.

2.1.3 Stress intensity factor

The stress intensity factor (K) is a dimensionless integer that quantifies the stress intensity at the crack tip. It is the result of the combined effect of applied stress, fracture geometry, and material parameters. This formulation has more usage when it is compared stress concentration factor. It is found by Irwin in 1960s and it is based on Griffith's Energy Criterion. [3] The formula that Irwin suggested:

$$K = \sigma\sqrt{(\pi a)} \tag{2.5}$$

where K is stress intensity factor, σ is stress value on the specimen, a is the half crack length on structure.

2.1.3.1 Loading modes of fracture

In general, there are three different loading modes that a crack can propagate under different loading types. In Figure 2.2, three different loading modes can be seen.[12]

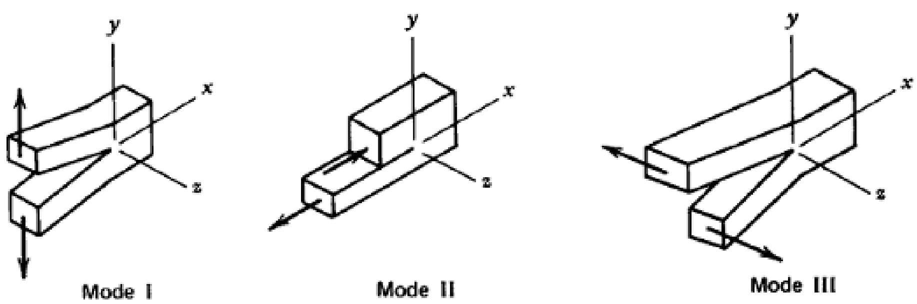

Figure 2.2 : Loading mode types of a crack.

In the Figure 2.2, Mode I denoted by a is the opening mode of the crack. This type of loading mode is the most common in the fracture mechanics since this type of cracks cause the most significant damage to structures. In this mode, the structures go under the high tensile loadings which are perpendicular to the crack plane.

Mode II (Figure 2.2, b) can be identified as sliding mode. In this mode, the shear forces are active and affect the structure as shearing due to in-plane stresses.

Mode III (Figure 2.2 c) is known as the tearing or anti-plane shear mode. In this mode, the part is under the loading of shear loadings in the perpendicular plane to the crack plane.

In the ideal world, it is assumed that a structure may be under the loading type separately in order to obtain governing equations of the crack growth. In a assumption like this, the most dangerous and effective type of the loading may be selected as Mode I. However, a combination of the loading types might create a situation which may lead a catastrophic failure.

In the Figure 2.3, a polar coordinate system is defined in order to represent stress tensor components in the crack tip. [13]

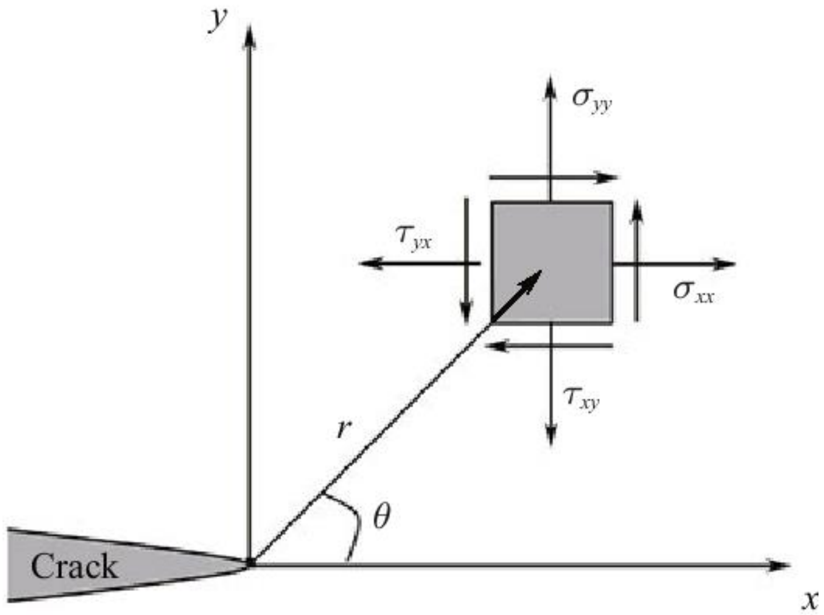

Figure 2.3 : Tensor component representation on the crack tip.

Where r and θ are the polar coordinate components and $\boldsymbol{\sigma_{xx}}, \boldsymbol{\sigma_{yy}}, \boldsymbol{\tau_{xy}}$ are stress components. In this system, the stress components can be achieved by following formulas generated by tensor mechanics and linear elasticity formulations:

$$\sigma_{xx} = \frac{K_I}{\sqrt{2\pi r}} \cdot \cos\left(\frac{\theta}{2}\right)\left[1 - \sin\left(\frac{\theta}{2}\right) \cdot \sin\left(\frac{3\theta}{2}\right)\right] \tag{2.6}$$

$$\sigma_{yy} = \frac{K_I}{\sqrt{2\pi r}} \cdot \cos\left(\frac{\theta}{2}\right)\left[1 + \sin\left(\frac{\theta}{2}\right) \cdot \sin\left(\frac{3\theta}{2}\right)\right] \tag{2.7}$$

$$\tau_{xy} = \frac{K_I}{\sqrt{2\pi r}} \cdot \cos\left(\frac{\theta}{2}\right) \cdot \left(\sin\left(\frac{\theta}{2}\right)\right) \cdot \cos\left(\frac{3\theta}{2}\right) \tag{2.8}$$

where K_I is the stress intensity factor. By using Equations 2.6 through 2.8, the stress components could be calculated at the tip of the crack.

2.1.3.2 Geometric correction factor

In the fracture mechanics, the stress intensity factor is generated for a specific condition, a plate with center crack. However, Tada, Paris and Irwin released a study about a parameter named as geometric correction factor (β) in order to represent different types of geometries. [14] In this study, there are multiple approaches in terms of geometries to satisfy stress intensity factor formulation for different geometries.

If the geometric correction factor is introduced into the stress intensity factor formulation, the final version may be written as:

$$K_I = \beta\, \sigma \sqrt{(\pi a)} \tag{2.9}$$

where β is the geometric correction factor.

2.2 Elasto-Plastic Fracture Mechanics

Elasto-Plastic Fracture Mechanics is an extension of fracture mechanics that takes into account the impacts of both elastic and plastic behavior in materials with cracks or faults. It deals with conditions in which considerable plastic deformation occurs at the fracture tip, which deviates from the assumptions of Linear Elastic Fracture Mechanics (LEFM).

2.2.1 J-Integral

The J Integral is a mathematical concept which is valuable in crack studies to state the energy release rate at the tip of a crack in a material. It has a significant role in understanding and predicting the propagation of crack and fractures in the geometries. This term is particularly important for scenarios where a material is affected by plastic deformation where the Hooke’s law is not applicable. [5]

J Integral can be written as follows for two directional applications:

$$\mathrm{J} = \int_{\Gamma} \mathrm{W}\,\mathrm{dy} - \mathrm{t}.\frac{\partial \mathrm{u}}{\mathrm{dx}}\mathrm{ds} \tag{2.10}$$

where W is strain energy density, u is the displacement field, s is the stress field. And the W strain energy density can be defined as:

$$\mathrm{W} = \int_{0}^{\varepsilon_{ij}} \sigma_{ij}.\,d\varepsilon_{ij} \tag{2.11}$$

where $\boldsymbol{\sigma_{ij}}$ and $\boldsymbol{\varepsilon_{ij}}$ are stress and strain tensor mechanics components, respectively.

Since J Integral is path independent and defined in an area which is far enough from the center crack, it can be calculated via linear formulations.

2.3 Paris-Erdogan Crack Propagation Law

Paris-Erdogan Law is the one of the most used crack propagation laws even though it presented in 1960 [4] This law states that there is a linear proportional region as stated in the figure as region 2 where stress intensity factor and the rate of the fatigue crack growth can be addressed in terms of each other.

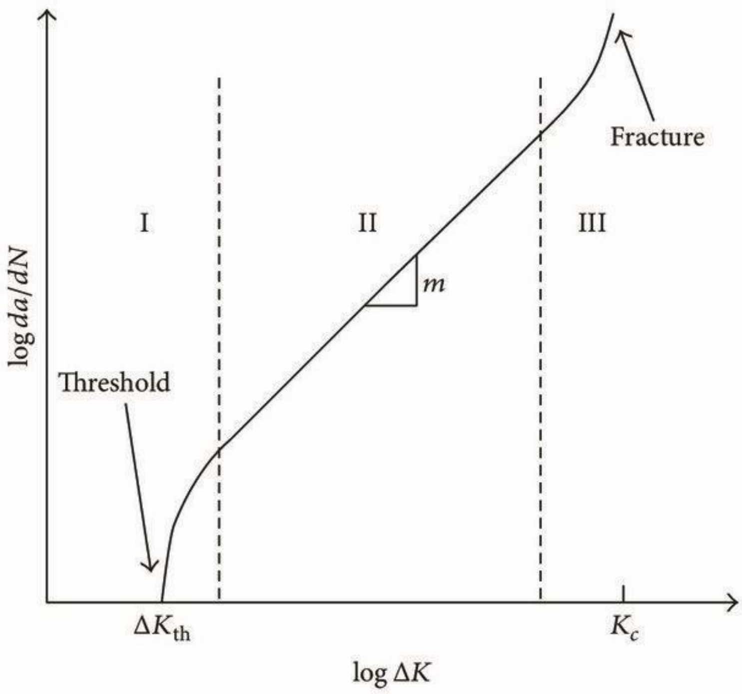

Figure 2.4 : Fatigue crack growth rate.

The Paris Erdogan's Law Equation can be written down as follows:

$$\frac{da}{dN} = C\,(\Delta K)^m \tag{2.12}$$

Where da/dN is the crack growth rate, $\Delta \boldsymbol{K}$ is the stress intensity range, C and m are the material related constants especial the Paris Equation.

If, the stress intensity factor is introduced as in the equation

$$\Delta K = \beta\,\Delta\sigma\sqrt{(\pi a)} \tag{2.13}$$

and replaced into the equation, the fatigue life cycle can be calculated by integrating final formula as:

$$N_{cycles} = \frac{2}{(2-m)\,C\big(\beta\,\Delta\sigma\sqrt{\pi}\big)^m}\,[a_c^{\frac{2-m}{2}} - a_i^{\frac{2-m}{2}}] \tag{2.14}$$

where a_c is the critical crack length and a_i is the initial crack length.

By using the final equation, someone could calculate final cycle number of the propagation by using initial and final crack lengths.

2.4 Machine Learning and its Algorithms

In today's world standards, the machine learning algorithms are widely used in most sectors in order to create automation systems. These automation systems can reduce the computational time, cost of the systems and manpower to handle a work.

The machine learning can be defined as a subpart of the artificial intelligence that consists development of the algorithms in order to create a new path for computers to make decisions about a job. The machine learning algorithms focus on prediction algorithms by learning from previously available data.

Machine learning algorithms can be divided in three main categories as shown in the figure.

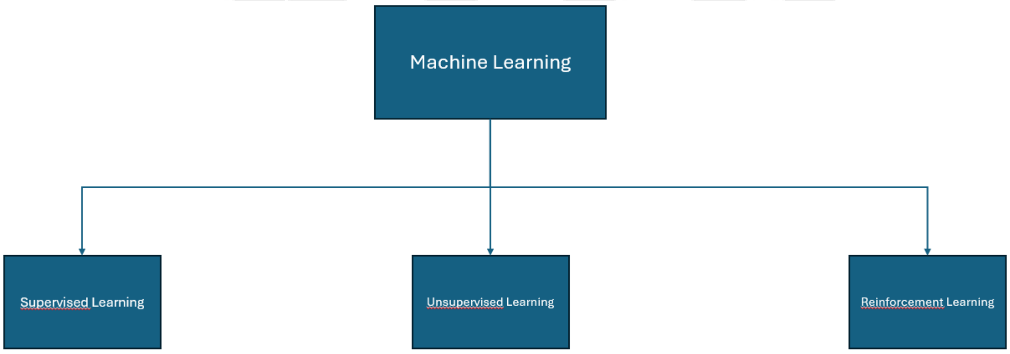

Figure 2.5 : Machine learning algorithms.

The supervised learning can be defined as a one of the machine learning algorithms that use already defined and labeled datasets for training itself. This type of machine learning code uses main mathematical fitting algorithms such as linear regression, polynomial regression until the given data and predicted data has a match.

The unsupervised learning is another machine learning algorithm that does not require data labeling. It uses different algorithms to capture similarities between given sets and creates its own labels to categorize the given data. This type of machine learning algorithms is widely used in image classification.

Finally, the reinforcement machine learning is a process of sequential events in order to make a decision as an autonomous system. In the reinforcement learning, a trial-and-error process are conducted in order to learn correct action to actualize a work without human interference.

3. NUMERICAL AND ANALYTICAL METHODS

In this section, the numerical and analytical methods of the fracture mechanics will be implemented.

In this thesis, the studies were made by starting from basic geometry such as compact tension specimen shown in Figure 3-1, to complex geometry which is a turbine blade geometry based from turbojet engine.

For methods, both of linear elastic fracture mechanics and elastic-plastic fracture mechanics were used where it is applicable. The main concern of using both methods is to verify FEM analysis with hand calculations.

Finally, a machine learning code is implemented into study for creating a user-friendly software for users who is not capable enough to study on Fracture Mechanics. The main goal of this part is to create a database from studies done via basic geometries in the first approach in order to get probabilistic results for requested geometry and load applications.

In this model, a user will enter their geometry properties such as first crack length, material, loading conditions, plate thickness etc. into machine learning interface and the software will scan its current database which was created by first approach in this study. After that, it will give requested results such as J Integral value, Stress Intensity Factor by using machine learning algorithms.

3.1 First Study: Compact Tension Test Specimen (CTT)

In the first study, a compact tension test specimen (CTT) was used in order to obtain a baseline for the machine learning algorithm which will be implemented further sections of this thesis.

In this study, the standard ASTM E399's Compact Tension Test Specimen shown in Figure was used[15].

Figure 3.1 : Compact tension test specimen.

The main usage of this specimen is to create a baseline in terms of fracture toughness of metallic materials by demonstrating various of tests in testing labs**.** These tests evaluate the material's resistance to fracture when cracks propagate perpendicular to the load. The specimen is a small, rectangular piece with a machined notch and a fatigue-cracked tip, simulating a natural crack. During testing, the specimen is loaded until it fractures, allowing calculation of critical value of the stress intensity factor. This value is crucial for understanding the material's behaviour in structural applications, especially where brittle fracture could lead to failure.

In the first section, a parametric study in terms of geometry and loading conditions are conducted by using CTT geometry as a baseline. Multiple test specimen geometries were studied by using both analytical and numerical methods in terms of LEFM and EPFM. Firstly, a geometry and a loading condition were selected to compare both analytical and numerical results. In following section, geometries, material properties and loading conditions will be implemented.

3.1.1 Compact Tension Test specimen geometry

According to ASTM E399-90[15], a test specimen is generally manufactured according to dimension parameters in Figure 3-2 in shown below. In this figure, W is the width of the specimen, a is the crack length, B is the specimen thickness.

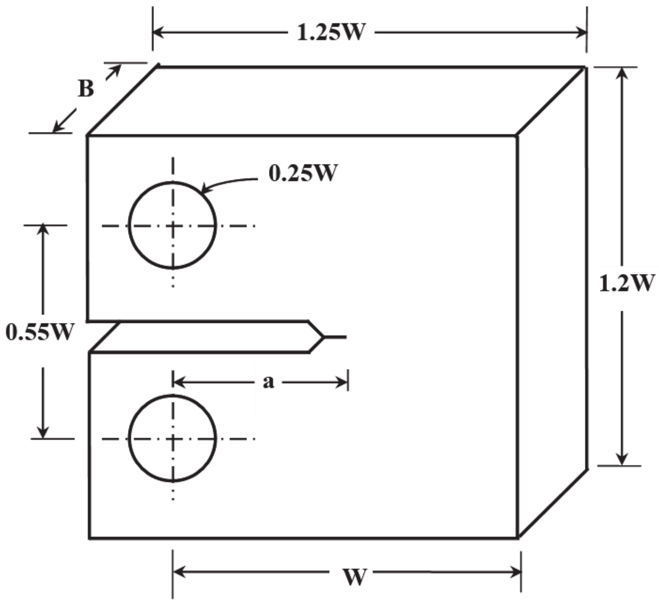

Figure 3.2 : Typical CTT parameters.

In order to calculate crack related factors by using numerical and analytical approaches, the geometric parameters a, W and B selected as 20mm, 50mm and 40mm, respectively. In further calculations, a, W and B dimensions were parametrized in order to obtain different geometric shapes to use in machine learning studies.

3.1.2 Analytical method

According to ASTM E399, a compact tension test (CTT) specimen should be manufactured according to formulation below in order to get valid values of K_{IC},

$$\text{B and a} \geq 2.5\left(\frac{K_{Ic}}{S_{TY}}\right) \tag{3.1}$$

$$0.45 \leq \frac{a}{W} \leq 0.55 \tag{3.2}$$

where W is the width of the specimen, a is the crack length, B is the specimen thickness, K_{Ic} is the critical stress intensity factor of the material and S_{TY} is the tensile yield strength of the material.

According to ASM database, Titanium Alloy Ti-6Al-4V has the fracture toughness around 95 MPa*m^0.5 and the given yield strength of 845.7 MPa. If the formulation in Equation 3.3 is calculated for these values:

$$B \text{ and } a \geq 2.5\left(\frac{K_{Ic}}{S_{TY}}\right) \rightarrow B \text{ and } a \geq 31.54 \text{ mm} \qquad (3.3)$$

It is seen that B and a value must be greater than 31.54 mm for Titanium Alloy Ti-6Al-4V in order to represent plane-strain intensity factor correctly.

Also, according to ASTM E399, the stress intensity factor around the tip can be calculated via the Equations below:

$$K_I = \frac{P}{B\sqrt{W}} \cdot f\left(\frac{a}{W}\right) \qquad (3.4)$$

Where

$$f\left(\frac{a}{W}\right) = \left(2 + \frac{a}{W}\right)\left[0.866 + 4.64\frac{a}{W} - 13.32\frac{a^2}{W} + 14.72\frac{a^3}{W} - 5.6\frac{a^4}{W}\right] \qquad (3.5)$$

where P is the tensile load, B is the specimen thickness, a is the crack tip length and W is the specimen width.

In order to calculate values, a python code was written to calculate stress intensity factor of the test specimen.

3.1.3 Numerical analysis

In order to calculate stress intensity factor K_I, J Integral values by numerically for both elastic and plastic material model, a common wide used commercial Finite Element Method software, ANSYS Mechanical 2024 R1 was used. ANSYS Mechanical can provide elegance solutions in terms of mechanical problems in the world, as well as fracture mechanics. Since its crack propagation tool, ANSYS SMART Crack Growth and other features available, it was selected as FEM Tool in this thesis.

In a general FEM analysis in ANSYS, the workflow usually can be shown in the figure:

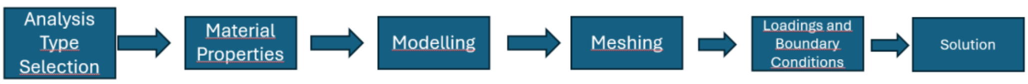

Figure 3.3 : Typical mesh flow in ANSYS.

3.1.3.1 Geometry

Firstly, both 2D and 3D geometries of CTT were drawn in ANSYS DesignModeler by using parameters stated in Section 3.1.1. The geometries can be shown below:

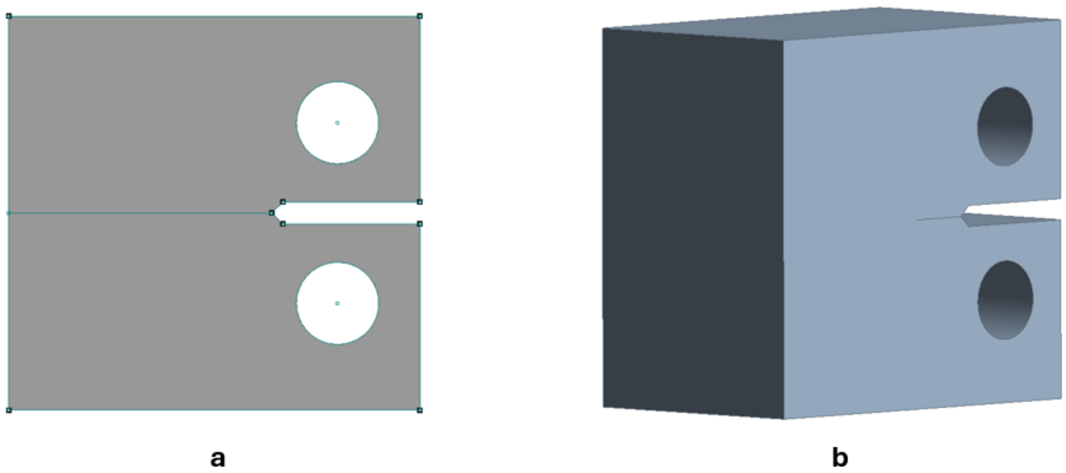

Figure 3.4 : 2D and 3D representation of CTT.

Since, both of geometries are symmetric with respect to middle plane of the structure, both geometries were cut into half in order to save mesh number and solution time. The final geometries which used in the analyses can be seen in figure.

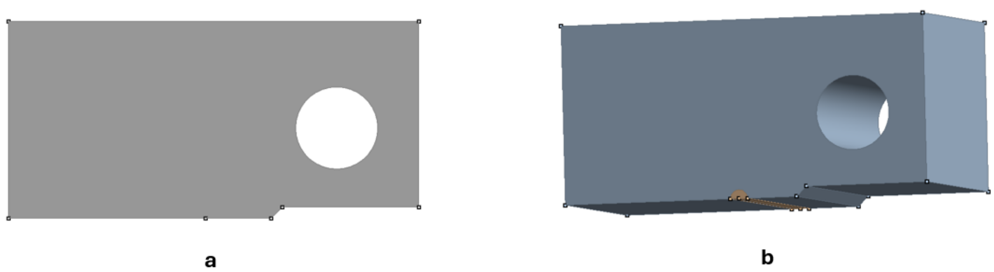

Figure 3.5 : Symmetric 2D and 3D geometries of CTT.

The analysis type was selected as whether 2D or 3D according to geometry dimensions.

3.1.3.2 Material

In this study, Titanium Alloy Ti-6Al-4V is selected as base material for CTT specimen. This material is widely used in aviation industry for its high strength, low weight and corrosion durability. It usually consists of %90 Titanium, %6 Aluminium and %4 Vanadium.

In the Table, physical and mechanical properties of Ti-6Al-4V is given as below:

Table 3.1 : Material properties of Ti-6Al-4V.

Density [kg.m^-3]	Young's Modulus [MPa]	Poisson's Ratio	Ultimate Tensile Strength [MPa]	Yield Tensile Strength [MPa]
4429	111200	0.3387	918	845.7

This material properties were gathered from ANSYS Granta Material Base, since this data can be used directly by selecting in ANSYS Mechanical.

However, it is required to have a plasticity model for Ti-6Al-4V in order to calculate its fracture mechanics values in Elasto-Plastic Fracture Mechanics. In this study, the plastic material properties of Ti-6Al-4V were calculated by using Ramberg-Osgood Equation and Neuber Correction formulation which are stated in Section 2.

If the Equation of Ramberg-Osgood is redeployed:

$$\varepsilon = \frac{\sigma}{E} + 0.002\left(\frac{\sigma}{S_{ty}}\right)^{n} \tag{3.6}$$

and n

$$n = \frac{ln\left(\frac{\varepsilon_{us}}{0.2}\right)}{ln\left(\frac{S_{tu}}{S_{ty}}\right)} \tag{3.7}$$

and ε_{us};

$$\varepsilon_{us} = 100\ (\varepsilon_r - \frac{S_{tu}}{E}) \tag{3.8}$$

where ε is the strain value, σ is the stress component, S_{ty} is the yield strength of the material, S_{tu} is the ultimate tensile strength and n is the Ramberg-Osgood coefficient and ε_{us} is the uniform strain value and ε_r is the maximum elongation of the material.

In order to approximate strain stress curve of Titanium Alloy Ti-6Al-4V, the material properties in Section 3.1.1.2 and the equations 3.4 and 3.5 will be used. If the maximum elongation of the material is taken as %0.2, the engineering stress-strain curve of can be drawn as in Figure:

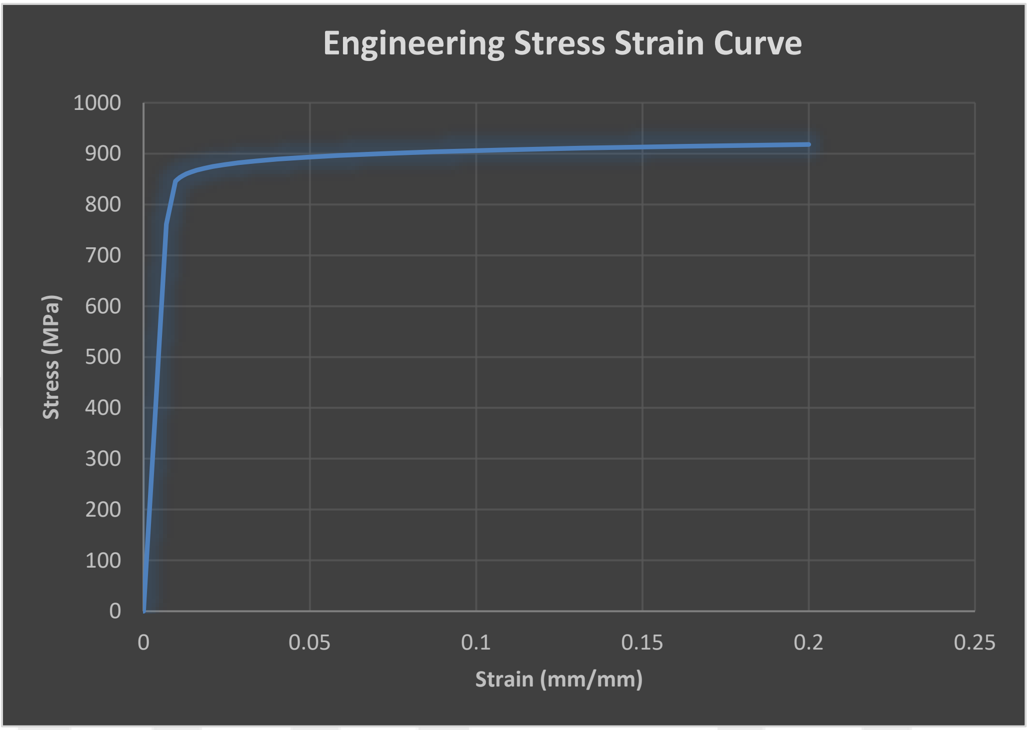

Figure 3.6 : Engineering stress-strain curve of Ti-6Al-4V.

Since, the figure consists of Engineering Stress-Strain Curve, someone needs to obtain true stress-strain curve in order to calculate plasticity effects on the material. The equations of through can be rewritten as:

$$\varepsilon_{True} = ln\,(1 + \varepsilon_{Engineering}) \tag{3.9}$$

$$\begin{aligned} \sigma_{True} &= \sigma_{Engineering} * e^{\varepsilon_{True}} \\ &= \sigma_{Engineering} * (1 + \varepsilon_{Engineering}) \end{aligned} \tag{3.10}$$

After deploying these equations, the true stress strain curve versus the engineering stress strain curve can be drawn as follows:

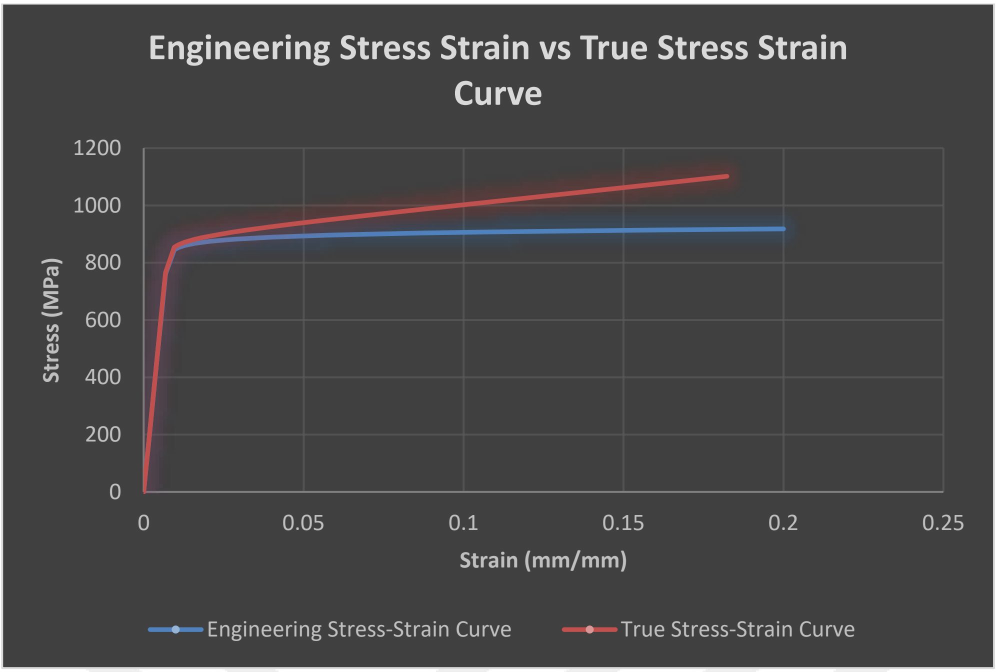

Figure 3.7 : Engineering stress strain vs true stress strain curve.

As it is seen in the figure, True Stress-Strain curve values are getting separated when high values of strain are obtained as expected. This situation occurs because, in contrast to engineering stress calculations, which only utilize the starting cross-sectional area, true stress calculations take into account the changing cross-sectional area at each time. The Poisson effect causes a material's cross-sectional area to shrink as it undergoes tensile deformation. Higher stress levels result from a reduction in area since stress is defined as force divided by area. True stress is therefore higher than engineering stress at large stresses.

Finally, it is required to gather the true plastic strain-true stress values as an input to ANSYS Mechanical in order to obtain plasticity model. If the equations are deployed:

$$\varepsilon_{Total,True} = \varepsilon_{Elastic,True} + \varepsilon_{Plastic,True} \tag{3.11}$$

$$\varepsilon_{Plastic,True} = \varepsilon_{Total,True} - ln\left(1 + \frac{\sigma_{Engineering}}{E}\right) \tag{3.12}$$

Finally, using the Equation 3.12, the true plastic strain-true stress values can be calculated as follows:

Table 3.2 : True plastic strain stress values of titanium alloy.

σ [MPa]	ε [mm/mm]
838.3698083	0
853.823131	0.001982937
857.9553146	0.00251317
862.2111595	0.003181757
866.6228904	0.004023839
871.2309524	0.005083193
876.0860605	0.006414263
881.251746	0.008084628
886.8075207	0.010177979
892.8528038	0.01279771
899.5117905	0.016071177
906.9394846	0.020154728
915.3291636	0.025239533
924.9216125	0.03155824
936.0165319	0.03939238
948.9866215	0.049080335
964.2949523	0.061025509
982.5163762	0.075704103
1004.363889	0.093671573
1030.721069	0.115566489
1062.681949	0.142110162
1101.6	0.174100051

These values will be used in the plastic analysis in order to calculate EPFM parameters. In this table, 853.82 MPa stress corresponds to material's Engineering Yield Strength point. After conversion to the true stress strain curve, it is accepted that there is no plastic strain occurs before this point.

3.1.3.3 Modelling

In the modeling section, two distinct approaches are considered: 2D modeling and 3D modeling. The primary objective of both modeling techniques is to accurately represent the 2D and 3D geometries, ensuring that the results obtained from each approach are comparable.

2D modeling

In 2D Modeling, the geometry behavior was selected as 2D Plane Stress with thickness elements. In the model, the thickness value stated in the beginning of the chapter of 40 mm was entered into model. Also, the material is selected as Titanium alloy, Ti-6Al-4V as shown in the figure.

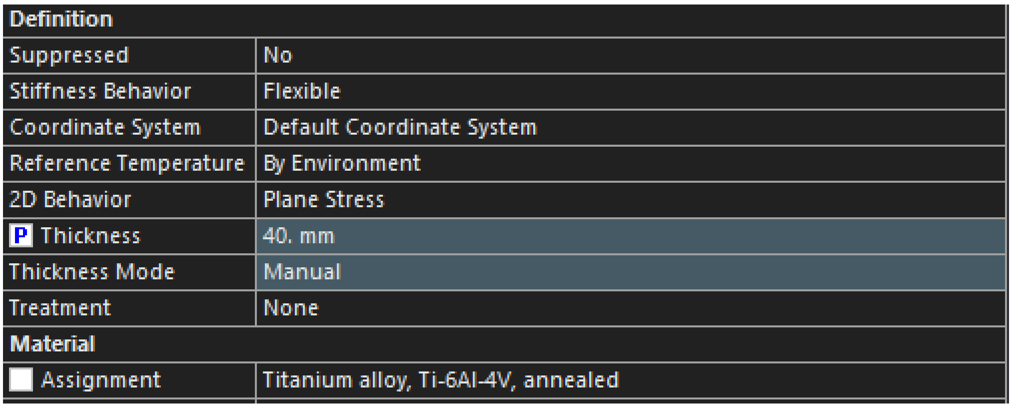

Definition	
Suppressed	No
Stiffness Behavior	Flexible
Coordinate System	Default Coordinate System
Reference Temperature	By Environment
2D Behavior	Plane Stress
P Thickness	40. mm
Thickness Mode	Manual
Treatment	None
Material	
Assignment	Titanium alloy, Ti-6Al-4V, annealed

Figure 3.8 : The geometric details of 2D model.

As it is stated before, the symmetry boundary condition was applied on the 2D geometry as shown in the figure

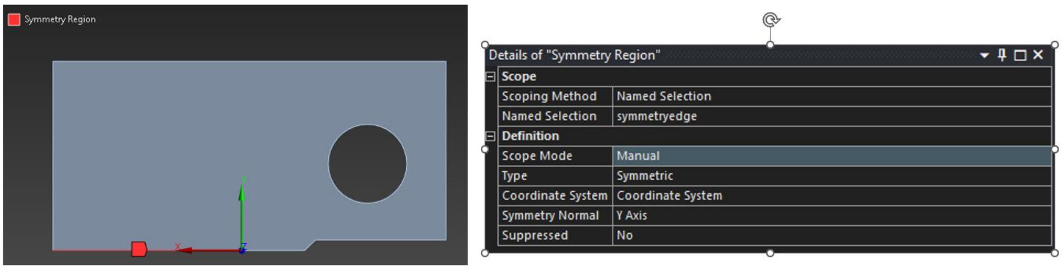

Figure 3.9 : Symmetry boundary condition.

The coordinate system located in the figure represents the crack tip location, therefore the symmetry edge shown by red edge were selected according to crack tip length.

In meshing section, PLANE183 2D- quadratic order mesh element was used in order to represent structure behaviour correctly. The global body size of 1.5 mm was selected for entire body. However, a vertex sizing of 0.05 mm was given at the region around the crack tip by using “Sphere of Influence” as seen in figure.

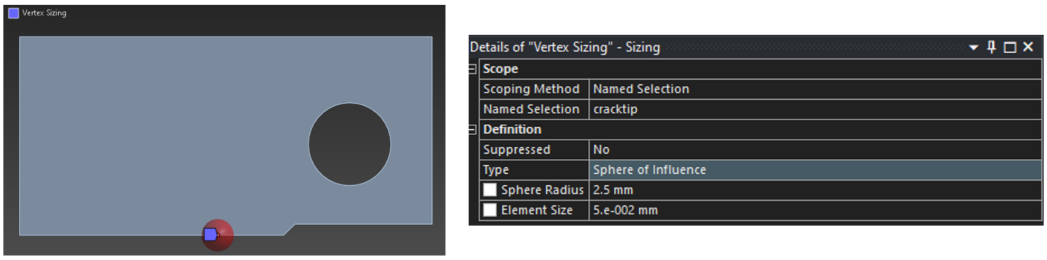

Figure 3.10 : The mesh refinement at the crack tip.

Final mesh can be seen in the figure with the total of 24096 nodes and 11912 elements.

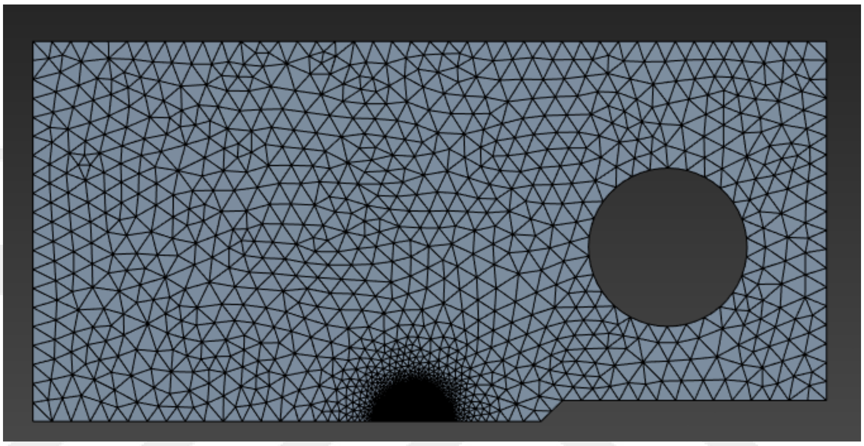

Figure 3.11 : Final mesh distribution of 2D geometry.

Furthermore, a pre-meshed crack feature was defined on the crack tip region. In this feature, the symmetry option was selected as "Yes" since the geomery was symmetric. The definition details can be seen as follows:

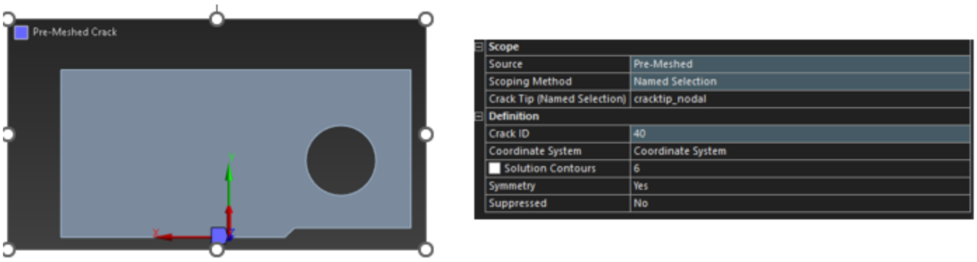

Figure 3.12 : Pre-meshed crack feature.

Finally, the remote force value of 10000 N and a displacement dof in y-direction were applied as in the testing procudure as seen in the figure.

Figure 3.13 : Boundary and loading conditions.

3D modelling

For 3D modelling, the 2D geometry was extruded for 40 mm in order to obtain 3D geometry. The same material model was used as 2D analysis stated in 2D Modelling section before.

In order to represent same behavior with respect to 2D Model, the same symmetry region condition was applied into model as shown in the figure.

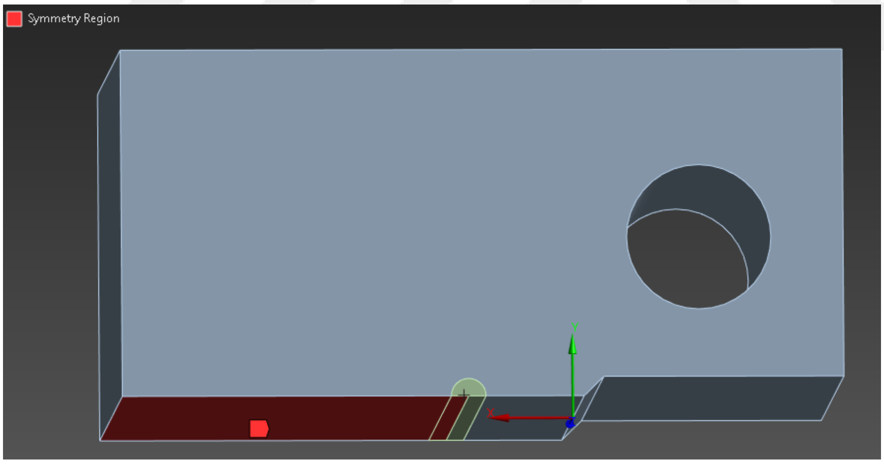

Figure 3.14 : Symmetry region of 3D model.

The geometry was meshed with the same approach as 2D Modelling with SOLID187 10 Node Tetrahedral Mesh Elements. A half cylinder area on the tip of the crack was separated in the geometry in order to have better mesh quality on the crack tip region. 0.15 mm was selected as body sizing for this region. The final mesh can be seen in the figure.

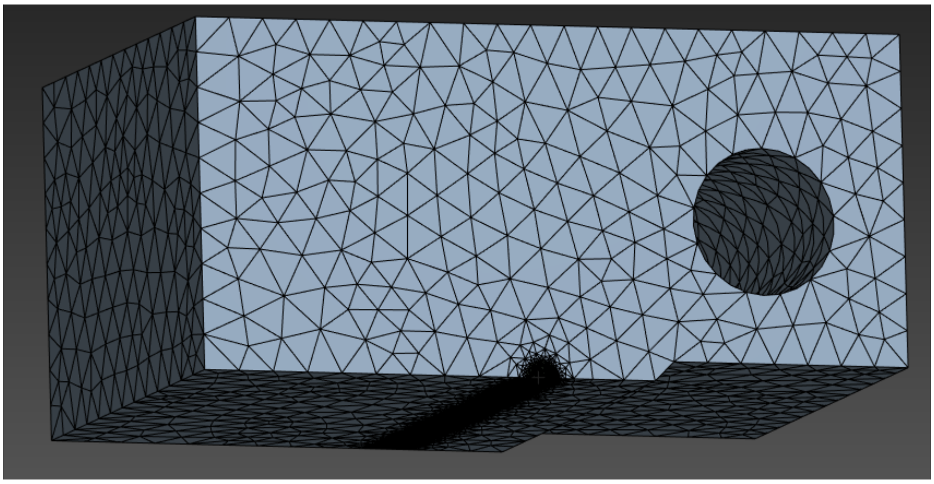

Figure 3.15 : Final mesh representation of 3D geometry.

Finally, the same boundary conditions and loads were applied into 3D Model as shown in the figure.

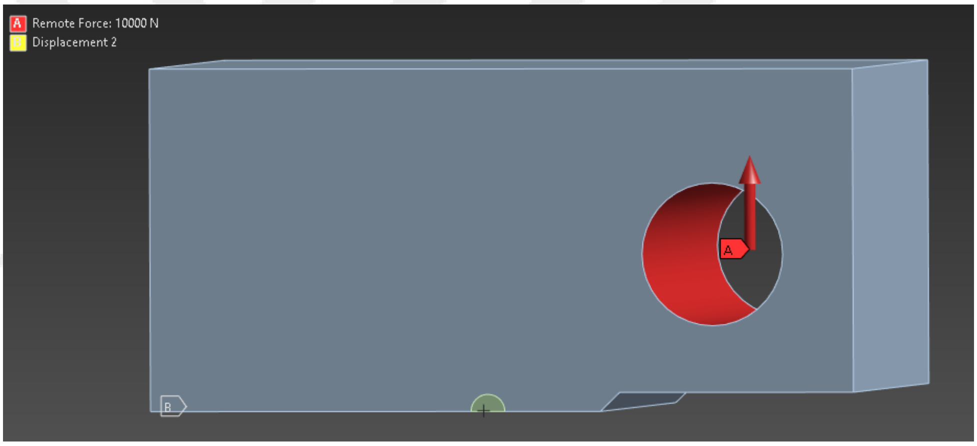

Figure 3.16 : Boundary condition and loading conditions of 3D model.

Moreover, 4 different type analyses (2D Elastic +2D Plastic, 3D Elastic + 3D Plastic) were conducted. The results of these analyses will be implemented in the Section 4.

3.2 Second Study: LEFM on a Turbine Blade of Turbojet Engine

In the second study, a turbine blade with firtree feature was analyzed according to principles of Linear Elastic Fracture Mechanics (LEFM).

3.2.1 The turbine geometry

The turbine geometry selection has a significant effect in terms of fatigue crack life since the geometric shapes may lead crack tip location with respect to blade geometry.

In the literature, there are various types of geometries according to their usage and performance criteria. As an example, The General Electric CF6 Engine is a widely used high bypass turbofan engine used in aviation. The high-pressure turbine blade of this engine can be seen in the Figure. [16]

Figure 3.17 : General Electric CF6 turbine blade.

As it is in the figure, the blade geometry has a male fir-tree structure in order to attach female fir-tree structures in the disc geometry. The fir-tree structure provides abilities of ease of disassembly, stress reduction at the connection points, thermal expansion accommodation.

An arbitrary turbine geometry with fir-tree structure was a created in the SOLIDWORKS CAD software by their wide usage in the aviation world. The geometry can be seen in the figure.

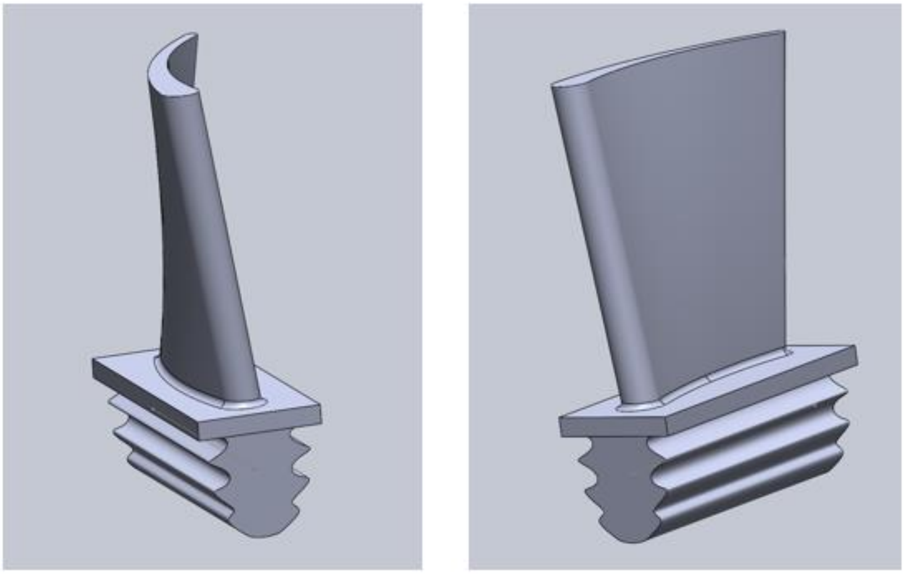

Figure 3.18 : 3D blade geometry drawn in SOLIDWORKS.

For the blade geometry, the NACA2424 airfoil was used as a base airfoil geometry section. After drawing the section profile, minor modifications were made and 3D blade geometry was drawn. Finally, an arbitrary fir-tree geometry was drawn as seen in the figure. Finally, the fillet radius of 1.5mm was added to root of the blade in order to have proper stress distribution.

3.2.2 Material

According to the book, “Turbines, Compressors, and Fans”, the materials generally used in gas turbines can be listed as in the table: [17]

Table 3.3 : Generally used gas turbine materials.

Cobalt-base and nickel base alloys	Metal matrix composites
Ceramics	Nimonic
Cromium-based alloys	Nickel powder alloys
Inconel	Super alloys
Titanium alloys	Stellite

According to this table, titanium alloy materials are also widely used in gas turbine engines. Therefore, Ti-6242 was selected as a base material for the turbine geometry.

Ti6242 are a widely used titanium alloy, which usually consists of %6 Aluminum, %2 Molybdenum, %88 Titanium and %4 Zirconium. The general application areas can be listed as high-temp jet engines, blades, discs and high-performance automotive valves. The material properties of Ti-6242 can be listed in the table below [18]:

Table 3.4 : Ti-6242 material properties.

Density [kg.m^-3]	Young's Modulus [MPa]	Poisson's Ratio	Ultimate Tensile Strength [MPa]	Yield Tensile Strength [MPa]
4540	120000	0.32	1010	990

Moreover, a typical FEM Software requires Paris-Erdoğan Law material constants for calculating fatigue crack growth. When the data available in the literature was checked, it is seen that there is an experimental study in order to obtain c and m values in the Paris Law. The values can be listed in the table as follows [19]:

Table 3.5 : Paris Law parameters of Ti-6242.

Material	Paris Parameters		Test Loading Type	Specimen
	m	C		
Ti 6242	3	1.90^-11	Pure Mode 1	SENT

3.2.3 Numerical analysis

In the numerical analysis of the turbine blade geometry, commercially available FEM Code ANSYS Mechanical 2024 R1 was used. In order to determine stress critical locations on the geometry, an elastic structural analysis was conducted. After the determination of the stress critical locations, a semi-elliptical crack was introduced into model to obtain fatigue crack growth parameters.

3.2.3.1 Elastic structural analysis

In this part, the geometry exported from SOLIDWORKS software was imported as Parasolid file into ANSYS SpaceClaim. In order to sustain well defined mesh, the geometry was chunked into sections stated by pink lines as shown in the figure.

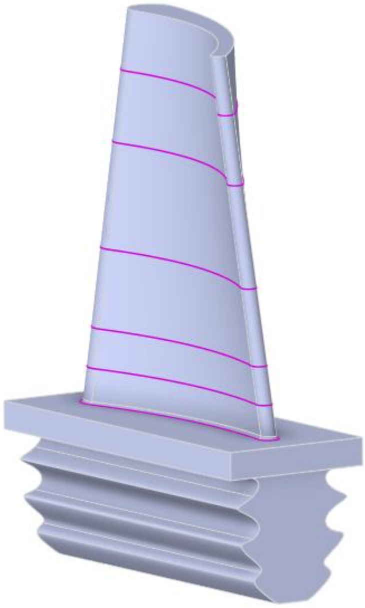

Figure 3.19 : Turbine geometry.

Modeling

After the geometry was imported to ANSYS Mechanical, the material assignment of Ti6242 was applied on the geometry.

In the meshing process, the general body size of the mesh was selected as 0.6mm. Since, the region above the platform section has higher possibility in terms of stress critical locations, SOLID186 20 Quadratic Node mesh elements were used. Moreover, the selected region in the figure has sweep mesh method in order to have aspect ratio of elements are closer to 1.

On the other hand, tetrahedral elements were used in the fir-tree region in order to reduce computational time for the analysis.

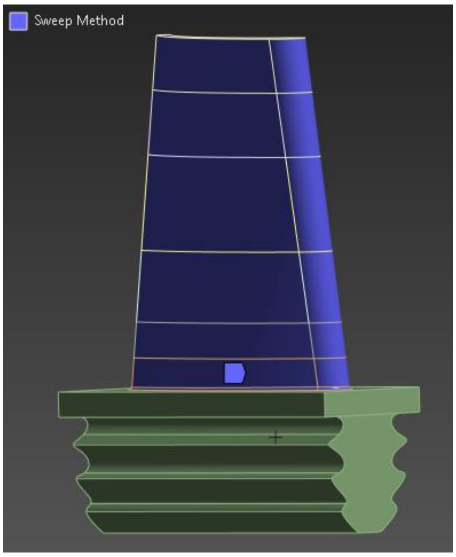

Figure 3.20 : Bodies with sweep mesh control.

The final mesh distribution can be seen in the figure. There were total of 313341 nodes and 90976 elements.

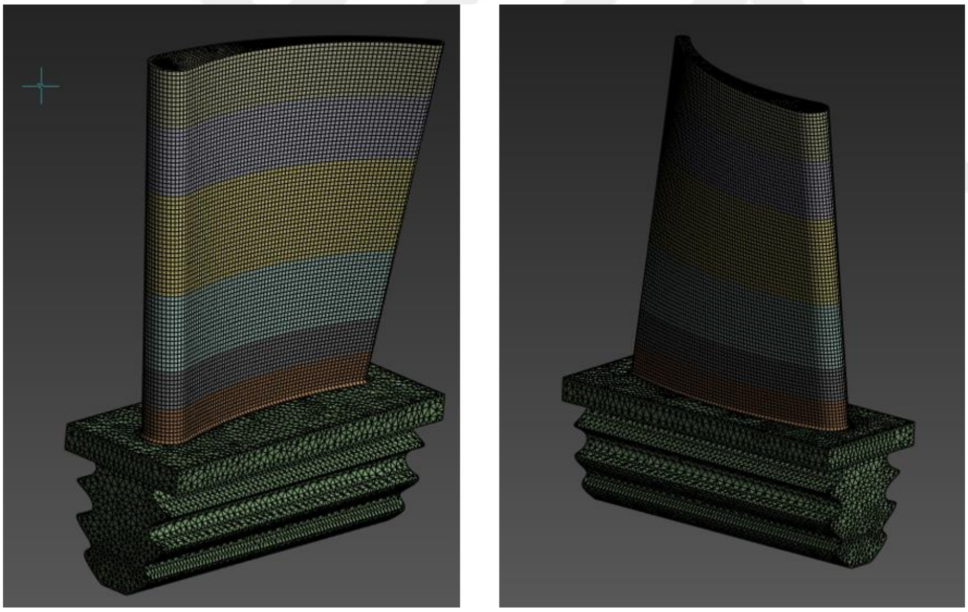

Figure 3.21 : Mesh distribution of turbine blade.

For the loading case, a rotational velocity of 20000 RPM value was given in order to represent centrifugal forces that blades of the turbine in a gas turbine engine are being subjected in operation condition.

Finally, the blade geometry has a boundary condition which are shown in the figure in order to represent contact situation between turbine disc and turbine blade. The fixed support was given to the faces which were designated as if contact faces.

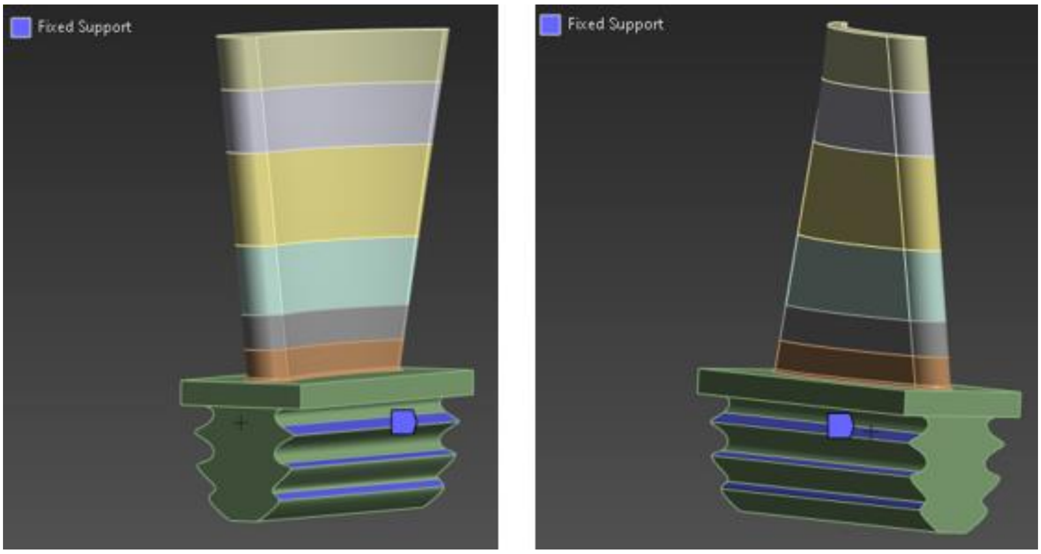

Figure 3.22 : Boundary condition of the turbine blade.

After, the boundary conditions and loading conditions were applied, the analysis was run in order to get equivalent Von-Mises stress and total deformation results.

Elastic structural analysis results

The total deformation, radial deformation and equivalent Von Mises stress results were achieved from ANSYS results. The relevant results can be seen in the figure 3-23 and 3-24, respectively.

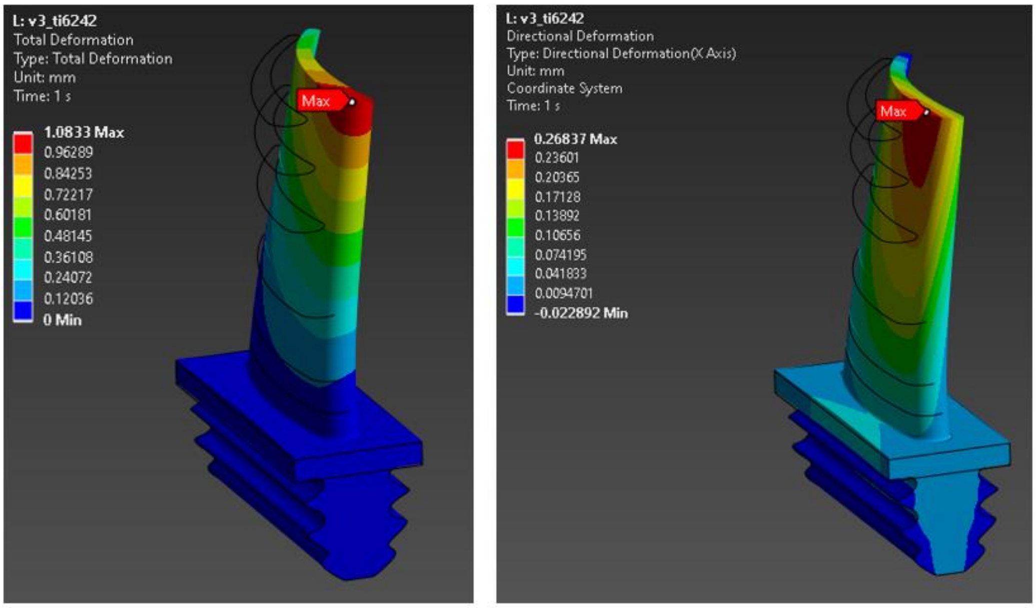

a b

Figure 3.23 : Total deformation and radial deformation of the turbine blade.

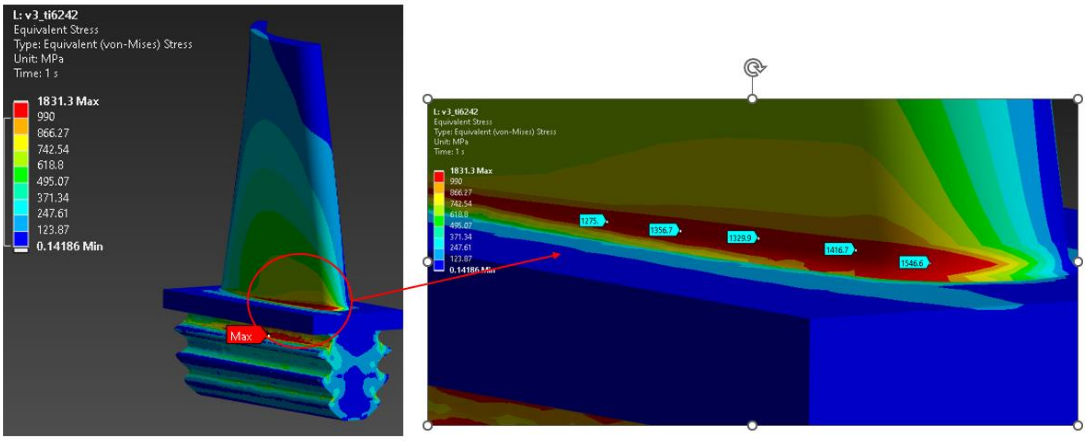

Figure 3.24 : Equivalent stress distribution of the turbine blade.

As it is seen in the figures, the maximum deformation was occurred on the tip of the blade with the value of 1.0833 mm. Moreover, in the figure, the equivalent Von-Mises Stress distribution was shown as the stress areas higher than the yield strength of the material 990 MPa were shown as red contours. The maximum equivalent Von-Mises Stress was occurred on the fir-tree region with the value of 1831.3 MPa. However, this stress value is not realistic since it is so close to fixed support boundary condition.

On the other hand, there was a high stress concentration region on the fillet radius of the suction side of the turbine blade which is shown in the figure. In further LEFM analysis, this area was selected as fracture critical region and further implementations have been done on this region.

3.2.3.2 LEFM on turbine geometry

After the determination of the stress critical regions on the turbine blade, a semi-elliptical crack model was assumed which were located on the leading edge of the blade geometry.

In order to save computational time, a basic blade geometry was drawn in SOLIDWORKS as shown in the figure:

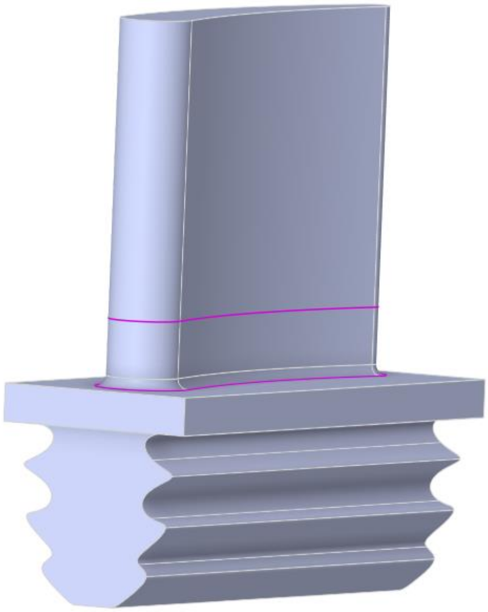

Figure 3.25 : Basic turbine blade geometry.

In ANSYS Mechanical, the same material model stated in Section 3.2.2 was used. In the leading-edge section, an initial semi elliptical crack model was assumed which was located near the stress critical locations determined in section 3.2.3.1.2. ANSYS SMART is able to create a crack mesh and update mesh around the crack tip when the crack propagates. The defined crack properties can be seen in the figure:

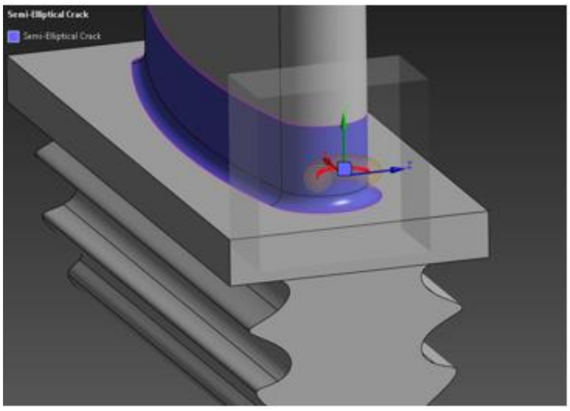

Scope	
Source	Analytical Crack
Scoping Method	Geometry Selection
Geometry	1 Body
Definition	
Crack ID	245
Coordinate System	Coordinate System 5
Align with Face Normal	No
Project to Nearest Surface	Yes
Crack Shape	Semi-Elliptical
--Major Radius	2. mm
--Minor Radius	2. mm
Mesh Method	Tetrahedrons
Largest Contour Radius	1. mm
Growth Rate	Default (1.2)
Front Element Size	Default (0.10071 mm)
Mesh Contours	6
Solution Contours	Match Mesh Contours
Suppressed	No
Buffer Zone Scale Factors	
X Scale Factor	2.
Y Scale Factor	2.
Z Scale Factor	2.
Named Selections Creation	
Crack Front Nodes	NS_SECrack_Front

Figure 3.26 : Crack definition of the turbine blade.

In general, the regions which are not the scope of the fracture mechanics, have the mesh body size control of 4 mm. The region which consists of the semi elliptical crack has the general body size of the 1 mm. Moreover, ANSYS SMART applied a mesh refinement on the crack tip nodes in order to represent crack propagation properly. The final mesh distribution is shown in the figure.

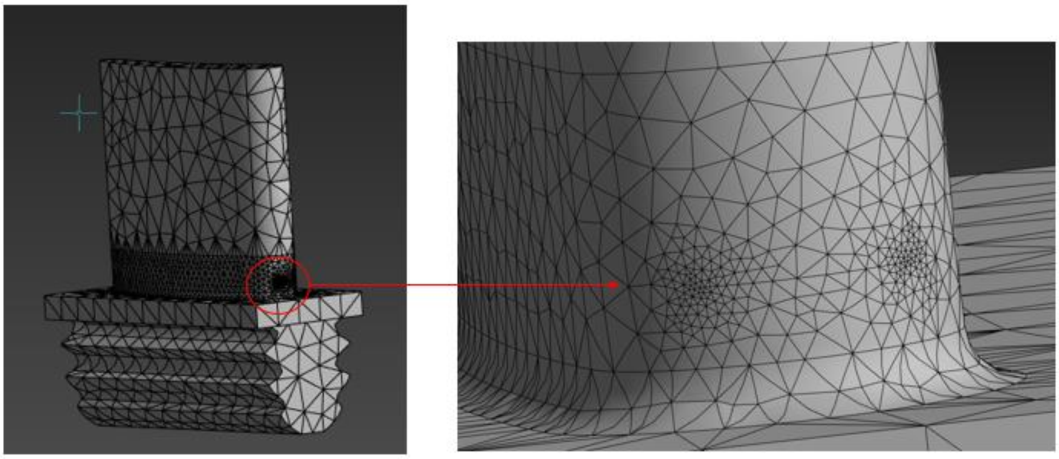

Figure 3.27 : Crack tip mesh refinement.

The same boundary conditions and loading conditions were applied in the elastic structural analysis stated before. The loading conditions can be seen in the figure.

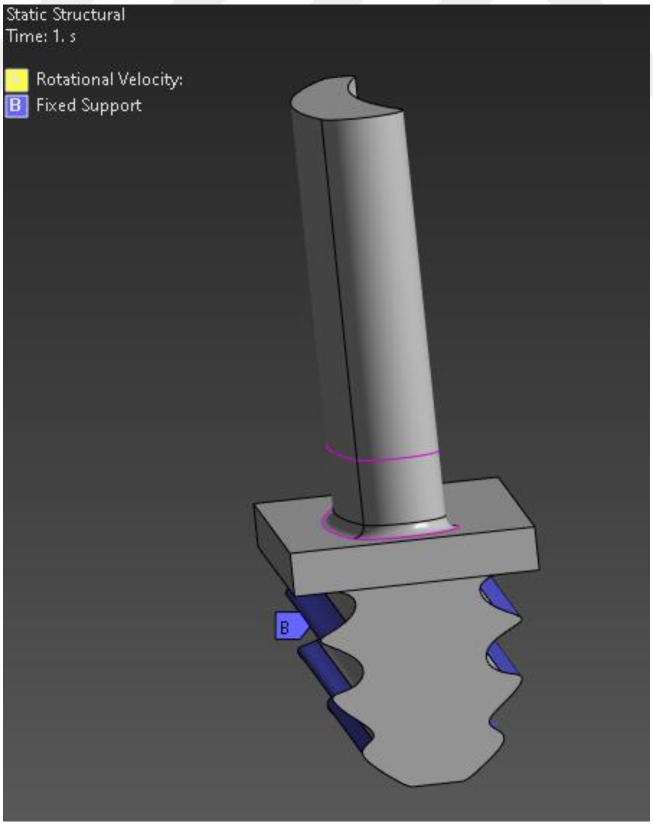

Figure 3.28 : Boundary condition and loading conditions of the turbine blade.

3.3 The Third Study: Machine Learning Algorithm for prediction of LEFM Parameters

In the first study, Linear Elastic Fracture Mechanics approaches were conducted on a Compact Tension Test Specimen under tensile loading. As 2D Model and the analytical solution has comparable results which are discussed in the Chapter 4, a machine learning model can be adapt to calculate different Linear Elastic Fracture Mechanics parameters such as Stress Intensity Factor and J Integral.

In order to create a database for the machine learning model, a parametric geometry of 2D Elastic CTT model was created in the ANSYS DesignModeler. The parametric values can be seen in the figure below:

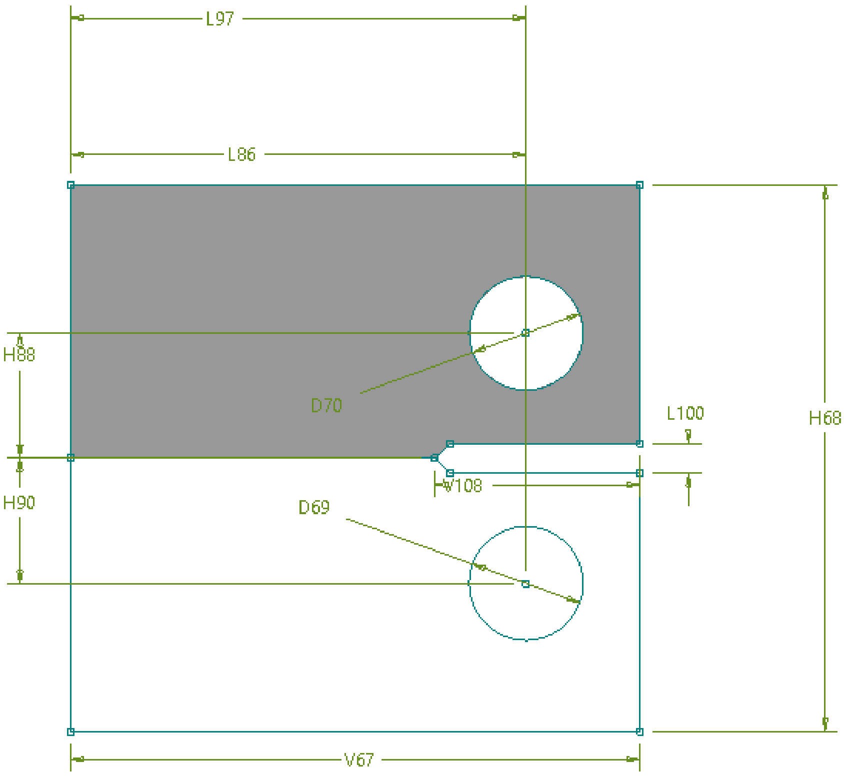

Figure 3.29 : Geomerty dimensions of 2D symmetric model.

Calculation parameters such as specimen width “W” and crack length “a” values are parametrized according to recommendation of ASTM E399 Test Standardization criteria as follows:

	Target	Expression	Type
✓	Plane4.H68	@W*1.2	Length
✓	Plane4.D70	@W*0.25	Length
✓	Plane4.D69	@W*0.25	Length
✓	Plane4.H88	@W*0.275	Length
✓	Plane4.V67	@W*1.25	Length
✓	Plane4.L100	@W/15	Length
✓	Plane4.H90	@W*0.275	Length
✓	Plane4.L86	@W	Length
✓	Plane4.L97	@W	Length
✓	Plane4.V108	@W*0.45	Length
✓	EdgeSplit4.FD2	@a-@W*0.20	Length

Figure 3.30 : Parametric equation of 2D symmetric model

After creating the geometry for different parameters, the Linear Elastic Fracture Mechanics parameters such as Stress Intensity Factor and J Integral values from the solution were also defined as output parameters as shown in the figure.

A	B
ID	Parameter Name
Input Parameters	
2d_iteration_first_run (A1)	
P19	a
P20	W
P23	Remote Force X Component
P29	Surface Body Thickness
New input parameter	New name
Output Parameters	
2d_iteration_first_run (A1)	
P21	SIFS (K1) Maximum
P22	Equivalent Stress Maximum
P30	Equivalent Plastic Strain Maximum
P31	J-Integral (JINT) Maximum

Figure 3.31 : Parametric input and output values in ANSYS Mechanical.

Finally, a random dataset of crack length a, specimen width W, specimen loading P and specimen thickness B were introduced into the ANSYS Mechanical in order to gather Stress Intensity Factor and J Integral and Equivalent Stress values numerically. This dataset consists of 235 different combinations of the geometric parameters. This dataset can be seen in the Appendix. This dataset was used in further machine learning algorithm to estimate stress intensity factors.

3.3.1 The machine learning algorithm

In order to create a machine learning algorithm, the scikit-learn machine learning libraries were used. The scikit-learn is a user-friendly machine learning library that provides different algorithms for different approaches. In this approach, a linear regression method was used. The main goal of this algorithm is estimating stress intensity factor by using the geometric parameters stated in the previous section.

Firstly, the database gathered from ANSYS Mechanical Analysis was saved as a csv file named ‘analysis_results.csv’.

Moreover, the stress intensity factors were separated from the dataset as y values whereas the other geometric and loading parameters were separated as x values in the machine learning model.

After that, the dataset should be divided into two different groups: training dataset and testing dataset. Usually, 0.2 test size is commonly used in the machine learning algorithms. This means that training set consists of %80 of all datasets and test set only has %20 percentage of the dataset. The training dataset was created by using sklearn’s train_test_split function. At the end, 188 rows of data were selected as training dataset and 47 rows of data were selected as test dataset.

In order to understand the distribution of the stress intensity factor in the database, a graph was drawn from all y values as shown in the figure:

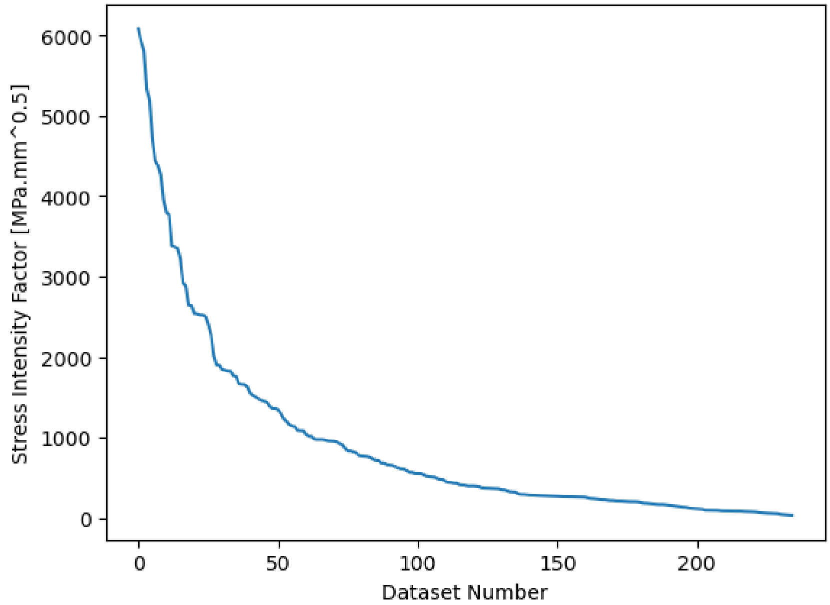

Figure 3.32 : Stress intensity factor curve.

As it is seen in the figure that the data distribution of the stress intensity factor creates an exponential curve. Generally, this kind of dataset requires a transformation of logarithmic function in order to calculate values with linear regression model.

After applying logarithmic transformation by using np.log function to all y values in the dataset, the current values can be drawn as follows:

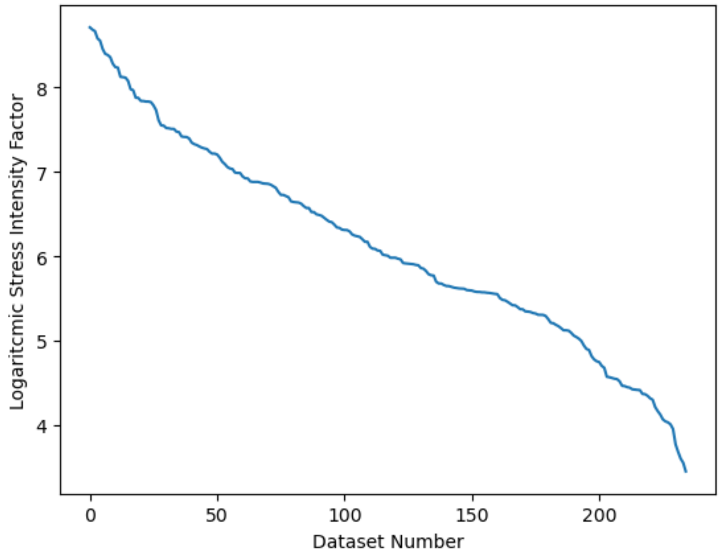

Figure 3.33 : Logarithmic stress intensity factor values.

After application of the logarithmic function to the dataset, the curve behavior can be represented by using linear regression method. This function can be imported by using following command line in the figure:

```
[14]: from sklearn.linear_model import LinearRegression
      lr= LinearRegression()
      lr.fit(x_train,y_train)

[14]: LinearRegression
      LinearRegression()
```

Figure 3.34 : Linear regression command line.

Finally, a result prediction in terms of stress intensity factor can actualized by using the command line bellow:

```
y_lr_train_pred = lr.predict(x_train)
y_lr_test_pred = lr.predict(x_test)
```

Figure 3.35 : Prediction function of the machine learning code.

The results of the prediction model are discussed in the Section 4.

4. RESULTS AND COMPARISON

4.1 First Study: Compact Tension Test Specimen (CTT) Results

4.1.1 The analytical results

If the stress intensity factor K_I formulation recalled from the section 3.1.2, the analytical solution for the CTT can be calculated via formulations below:

$$K_I = \frac{P}{B\sqrt{W}} \cdot f\left(\frac{a}{W}\right) \tag{4.1}$$

$$f\left(\frac{a}{W}\right) = \left(2 + \frac{a}{W}\right)\left[0.866 + 4.64\frac{a}{W} - 13.32\frac{a^2}{W} + 14.72\frac{a^3}{W} - 5.6\frac{a^4}{W}\right] \tag{4.2}$$

In the first study, the geometric parameters a, W and B selected as 20mm, 50mm and 40mm, respectively. And the loading force was taken as 10000 N. If these values were submitted into equations above, the stress intensity factor can be calculated via a python code:

$$K_{I_{analytical}} = 257.16\ MPa\sqrt{mm} \tag{4.3}$$

For the J Integral value, it is required to use formulation below:

$$J_{Total} = J_{Elastic} + J_{Plastic} \tag{4.4}$$

For the elastic J- Integral, it is equal to energy release state of the structure G stated in the formulation:

$$J_{Elastic} = G = \frac{K_I^2}{E'} \tag{4.5}$$

Where $\boldsymbol{E'}$ is equal to Young Modulus E for the plane stress conditions. By substitution of the required parameters in the equation, J- Elastic can be calculated as:

$$J_{Elastic} = G = \frac{K_I^2}{E'} = \frac{(257.16)^2}{111200} = 0.594682 \frac{mJ}{mm^2} \tag{4.6}$$

Finally, the plastic J-Integral value can be calculated as follows:

$$J_{Plastic} = \frac{\alpha\left(S_{ty}\right)^2 (W-a)}{E} * h_1\left(\frac{a}{W}, n\right) * \left(\frac{P}{P_0}\right)^{n+1} \tag{4.7}$$

where

$$P_0 = 1.455 * p * (W-a) * S_{ty} \text{ for plane strain} \tag{4.8}$$

$$P_0 = 1.071 * p * (W-a) * S_{ty} \text{ for plane stress} \tag{4.9}$$

and

$$p = \left[\left(2\frac{a}{(W-a)}\right)^2 + 2\left(\frac{a}{(W-a)}\right) + 2\right]^{0.5} - [2\left(\frac{a}{(W-a)}\right) + 1] \tag{4.10}$$

Where P is the applied load per unit thickness, a is the crack length, W is the specimen width, h_1 is a constant function of the a/W, α and n is the material constants.

4.1.2 Numerical solutions

From ANSYS Mechanical Results, the total deformation of the 2D and 3D geometry can be seen in the figures, respectively.

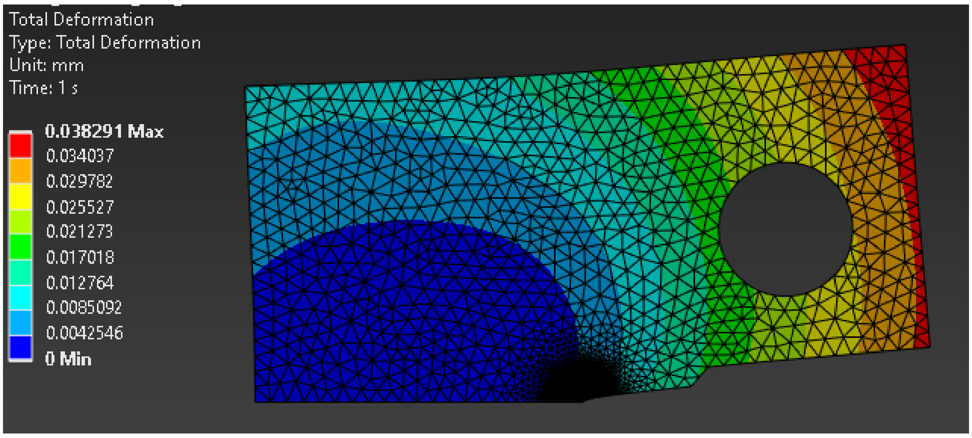

Figure 4.1 : 2D elastic analysis- total deformation.

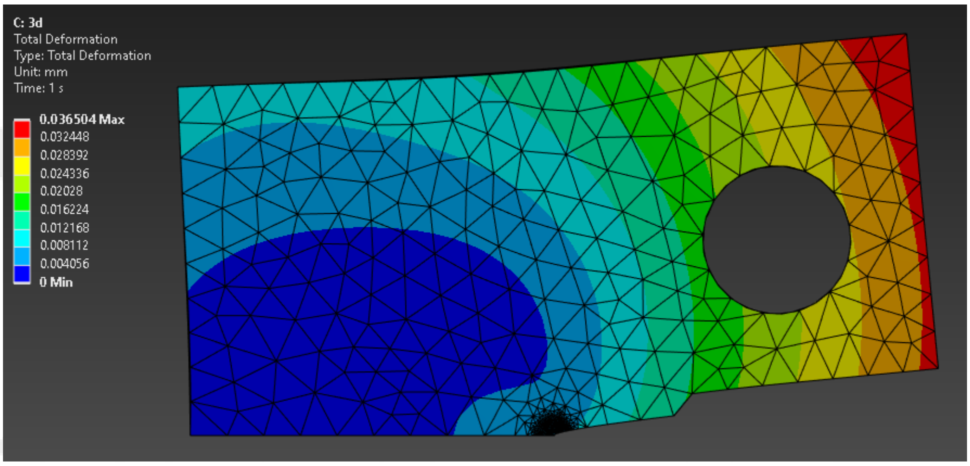

Figure 4.2 : 3D elastic analysis- total deformation.

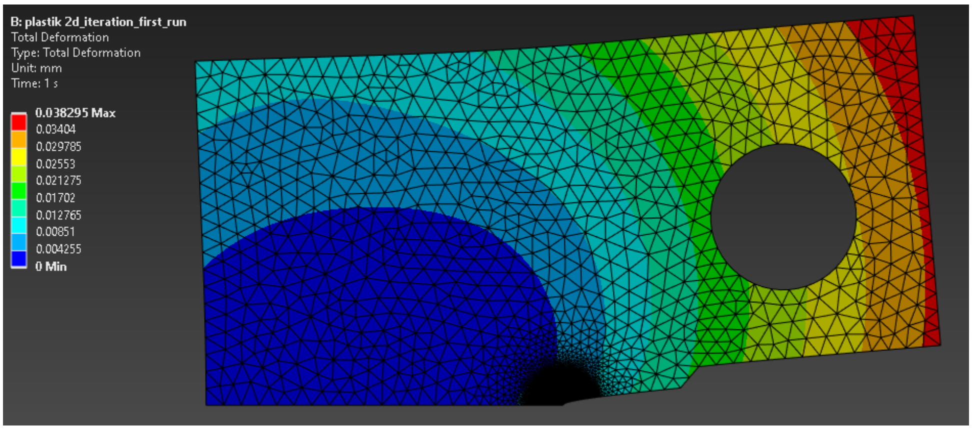

Figure 4.3 : 2D plastic analysis- total deformation.

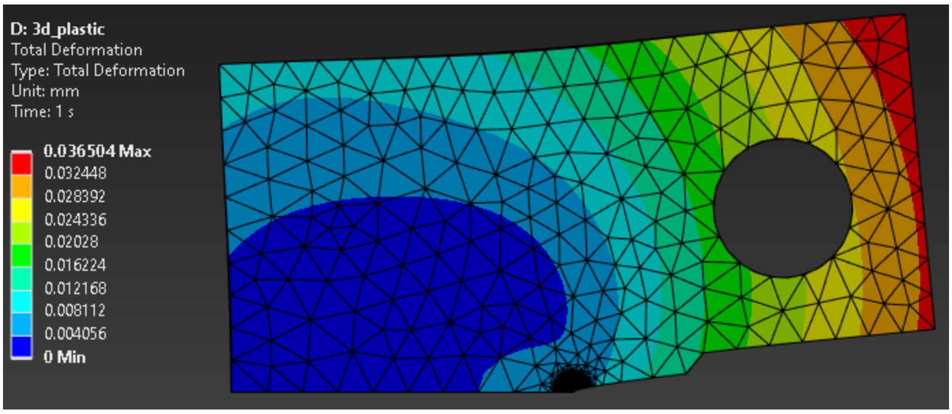

Figure 4.4 : 3D plastic analysis- total deformation.

As it is seen, the maximum total deformation value and the general contour distribution are consistent between 2D and 3D models.

4.1.2.1 Stress intensity factors

2D elastic model

In 2D Elastic Model, the maximum stress intensity factor K1 was calculated as 259.56 MPa.mm^0.5 as shown in the figure.

Figure 4.5 : The maximum stress intensity factor of 2d elastic model.

2D plastic model

In 2D Plastic Model, the maximum stress intensity factor K1 was calculated as 259.58 MPa.mm^0.5 as shown in the figure.

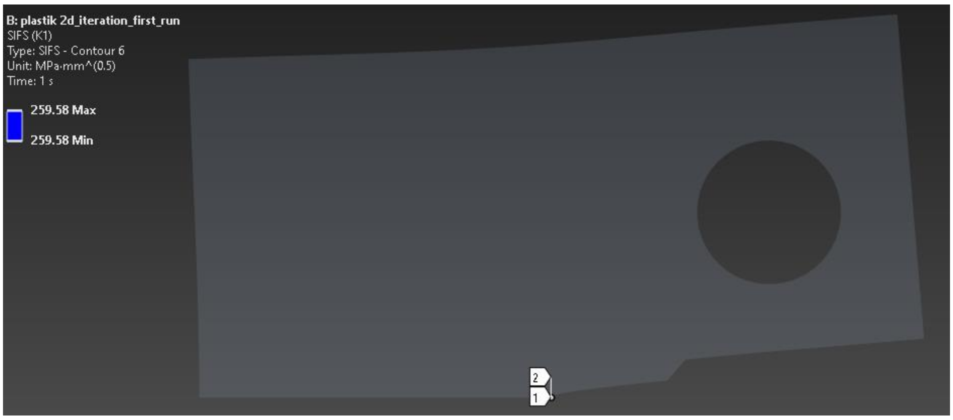

Figure 4.6 : The maximum stress intensity factor of 2d plastic model.

3D elastic model

In 3D Elastic Model, the maximum stress intensity factor K1 was calculated as 254.88 MPa.mm^0.5 as shown in the figure. Moreover, K1 distribution along the specimen thickness can be seen in the figure.

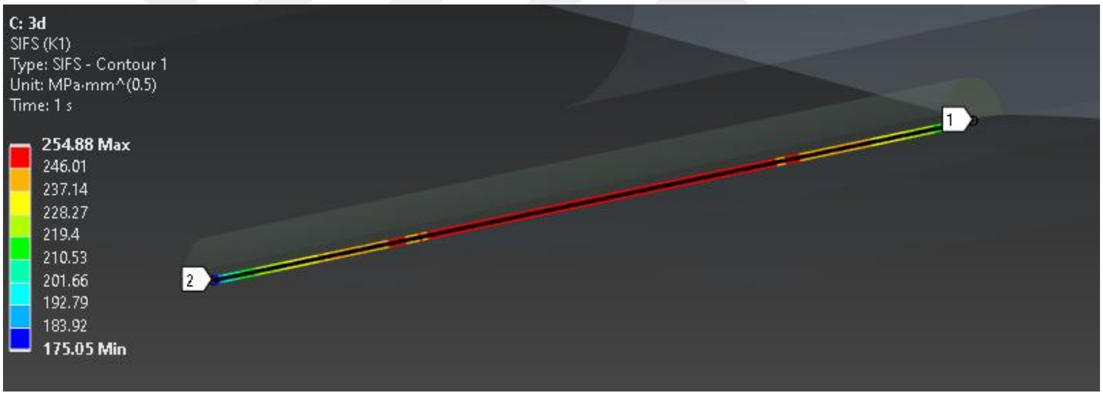

Figure 4.7 : Stress intensity factor distribution of 3d elastic model.

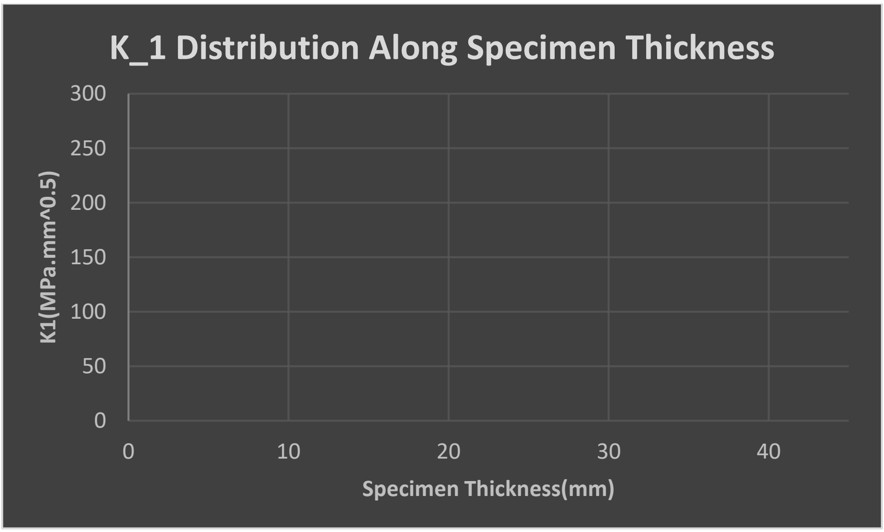

Figure 4.8 : K_1 distribution along specimen thickness.

3D plastic model

In 3D Plastic Model, the maximum stress intensity factor K1 was calculated as 255.09 MPa.mm^0.5 as shown in the figure. Moreover, K1 distribution along the specimen thickness can be seen in the figure.

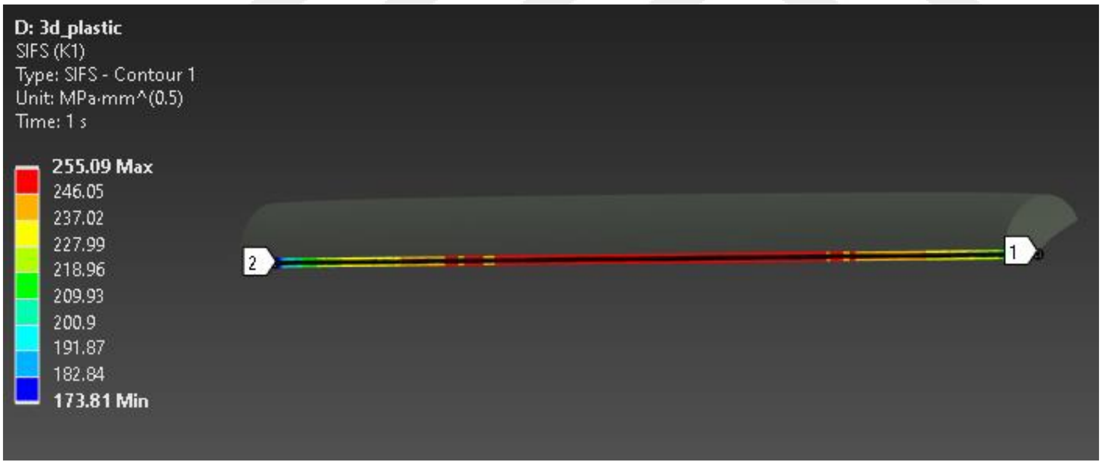

Figure 4.9 : Stress intensity factor distribution of 3d plastic model.

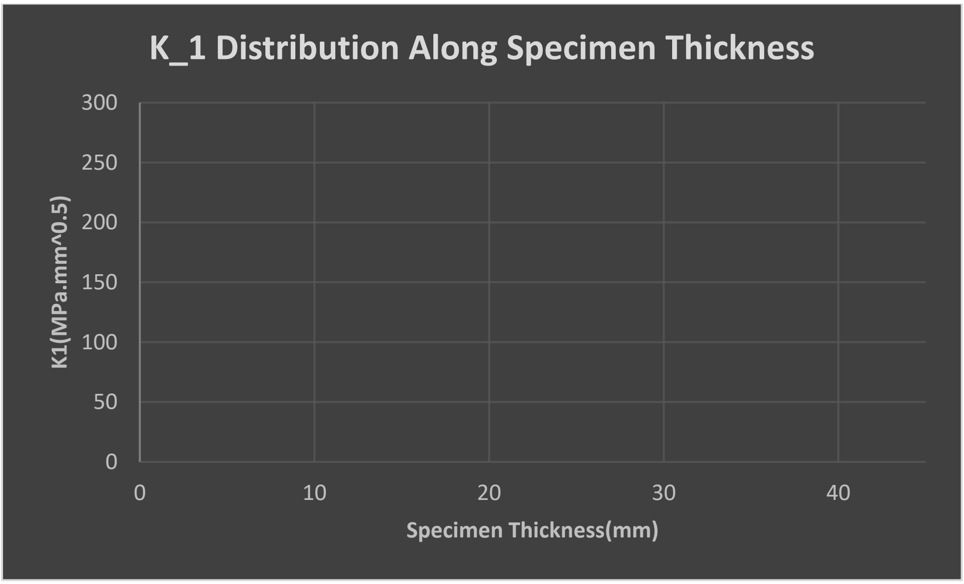

Figure 4.10 : K_1 distribution along specimen thickness.

As it is seen, the K1 stress intensity factors are consistent within all 2D Elastic-Plastic and 3D-Elastic Plastic analyses.

4.1.2.2 J integral results

2D elastic model

In 2D Elastic Model, the Elastic J Integral value was calculated as 0.60608 mJ/mm^2 as seen in the figure:

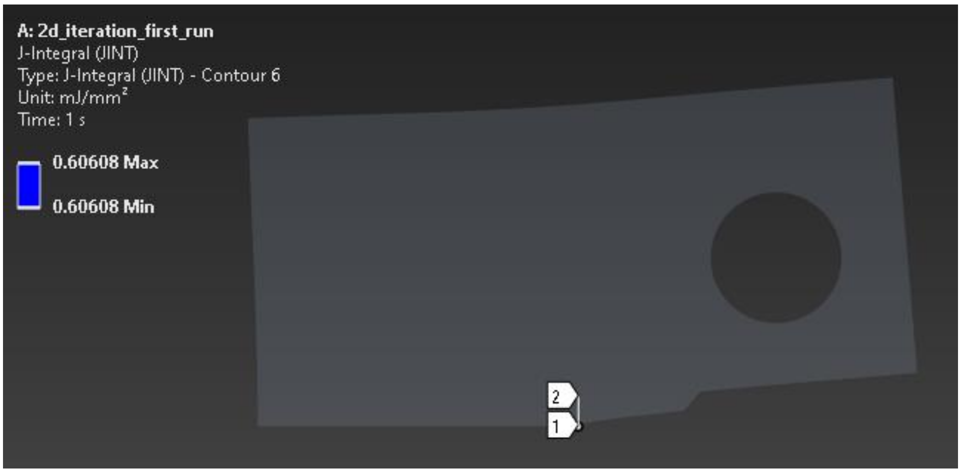

Figure 4.11 : Elastic J-Integral results of 2D elastic model.

2D plastic model

In 2D Plastic model, the total J Integral value was calculated as 0.60614 mJ/mm^2 as seen in the figure:

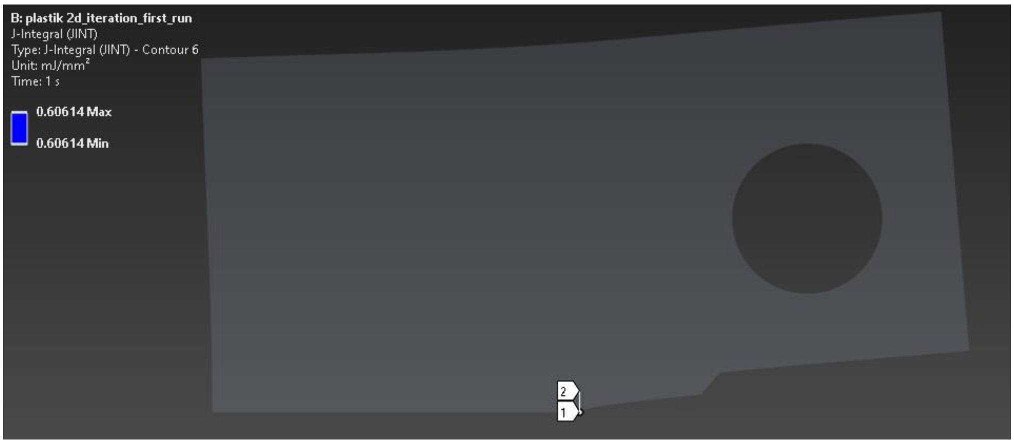

Figure 4.12 : Total J-Integral results of 2D plastic model.

3D elastic model

In 3D Elastic model, the elastic J Integral value was calculated as 0.64348 mJ/mm^2 as seen in the figure. Moreover, elastic J Integral distribution along the specimen thickness can be seen in the figure:

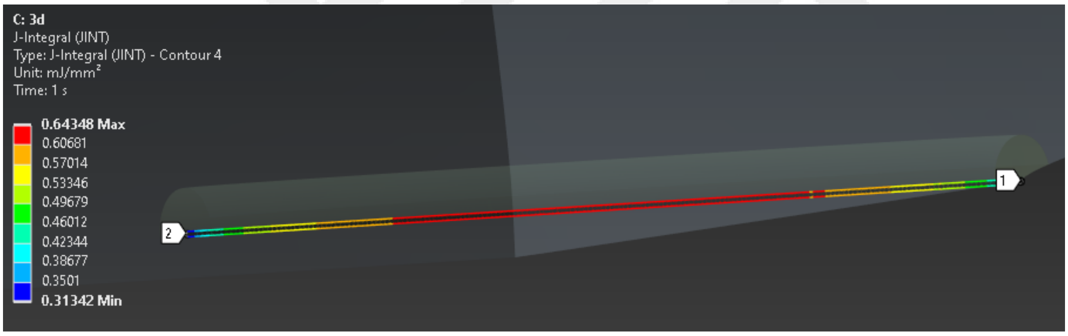

Figure 4.13 : Elastic J-Integral results of 3D elastic model.

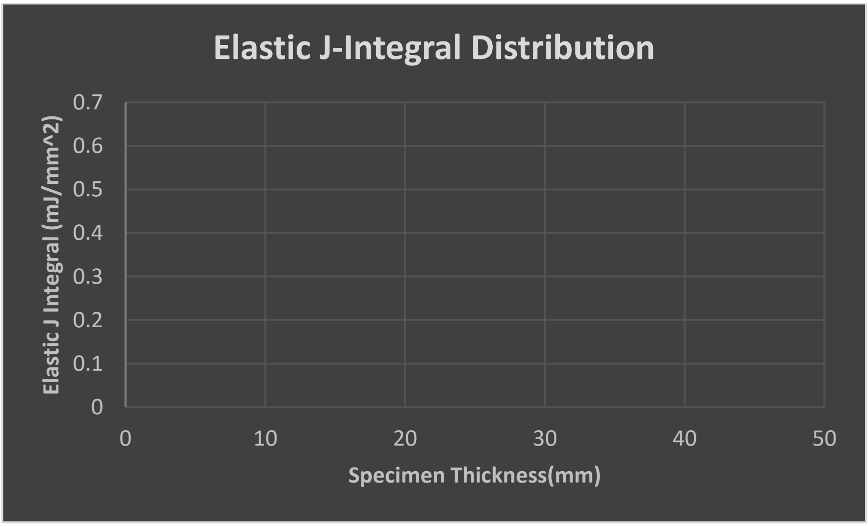

Figure 4.14 : Elastic J-Integral distribution of 3D elastic model.

3D plastic model

In 3D Plastic model, the total J Integral value was calculated as 0.64355 mJ/mm^2 as seen in the figure. Moreover, total J Integral distribution along the specimen thickness can be seen in the figure:

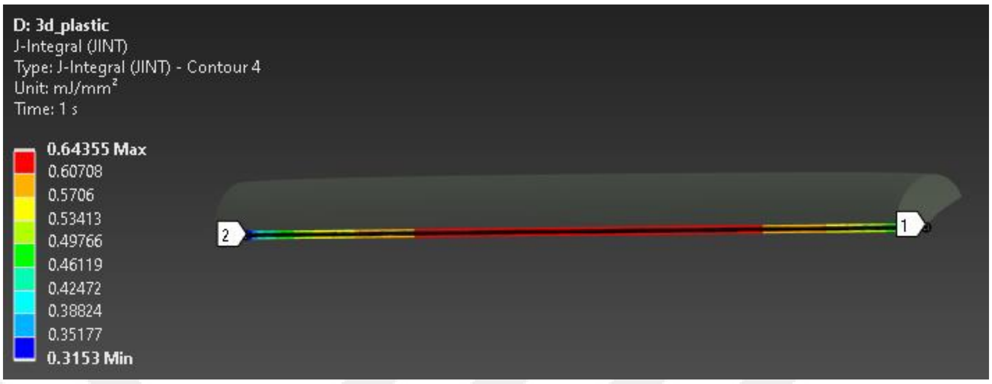

Figure 4.15 : Total J-Integral results of 3D plastic model.

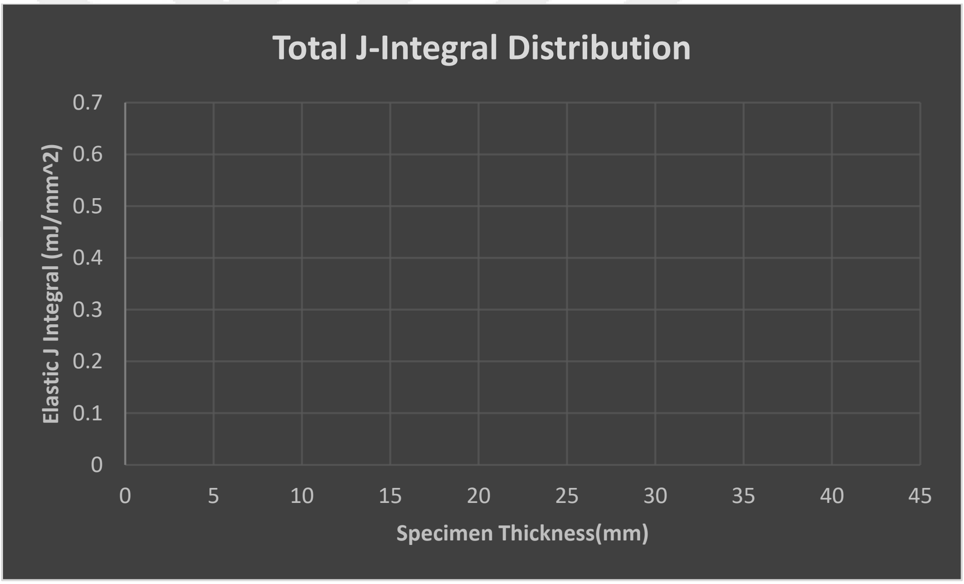

Figure 4.16 : Total J-Integral distribution of 3D plastic model.

4.1.2.3 Result comparison of stress intensity factor

The all results for Stress Intensity Factors were gathered together in the table below:

Table 4.1 : Stress intensity factors for all analyses.

Analytical Solution	2D Elastic Solution	2D Plastic Solution	3D Elastic Solution	3D Plastic Solution	Error-2D Elastic (%)	Error-2D Plastic (%)	Error-3D Elastic (%)	Error-3D Plastic (%)
257.16	259.56	259.58	254.88	255.09	0.933	0.941	0.887	0.805

In the table, the error calculation was made with respect to analytical solution. All the error percentages are lower than 1 percent. The calculation parameters and the analysis results are comparable with each other.

4.1.2.4 Result comparison of elastic j integral

The all-results for Elastic J Integral were gathered together in the table below:

Table 4.2 : Elastic J-Integral results for all analyses.

Analytical Solution	2D Elastic Solution	3D Elastic Solution	Error-2D Elastic (%)	Error-3D Elastic (%)
0.594682	0.60608	0.64348	1.916655	8.20573

In the table, the error calculation was made with respect to analytical solution. The error between 2D Elastic Analysis and Analytical solution is lower than the error between 3D Elastic Analysis. 3D Analysis error is approximately %8.2. This difference may be occurred due to coarse mesh in 3D Analysis and plane stress approximation.

Due to the results consistency, 2D Fracture models can be used in the machine learning study introduced in the Section 3.

4.2 Second Study: LEFM on a Turbine Blade

After all analysis were completed on the turbine blade geometry, the crack extension value at the end of the analysis was calculated as 9.5408 mm. The crack extension probe with respect to analysis time can be plotted as follows:

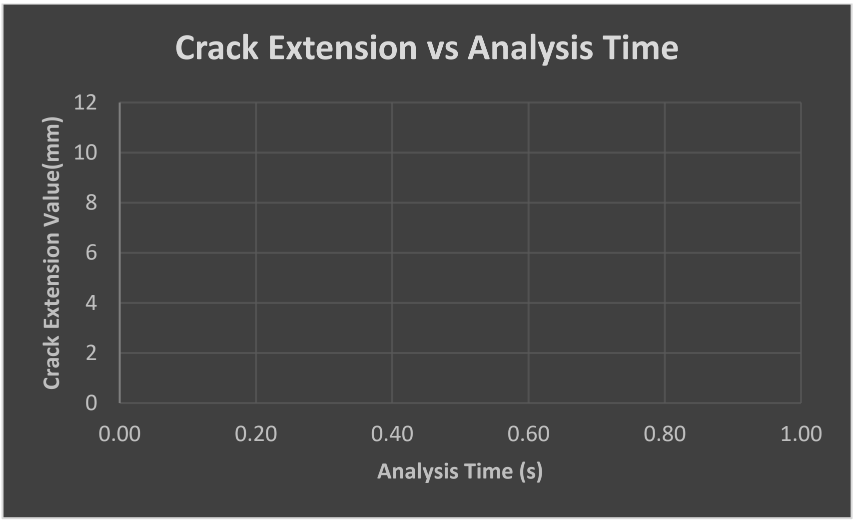

Figure 4.17 : Crack extension vs analysis time.

Moreover, it is calculated that 11753 cycles in order to crack propagates to the value of 9.5408 mm. The crack extension value versus total number of cycles graph can be seen in the figure below:

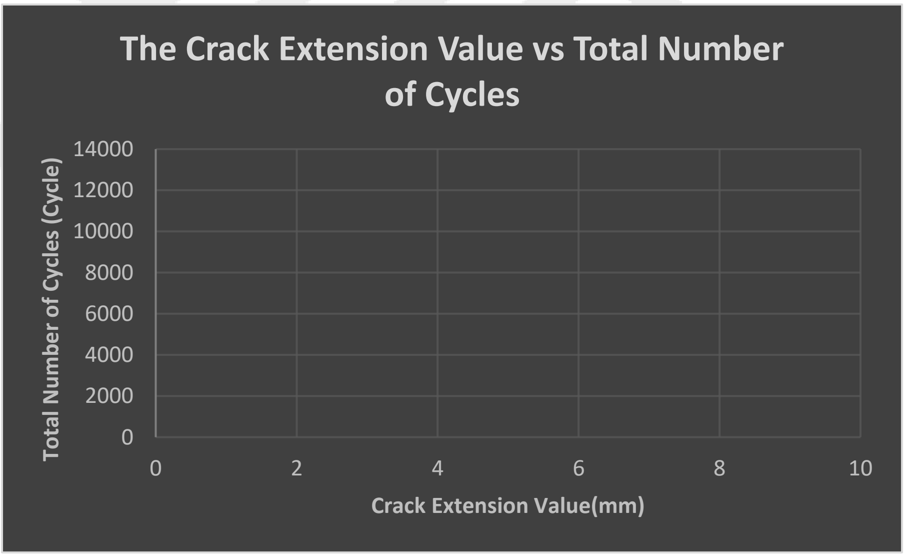

Figure 4.18 : The crack extension versus total number of cycles.

The total deformation result after crack propagation exaggerated for 50 times can be seen in the figure:

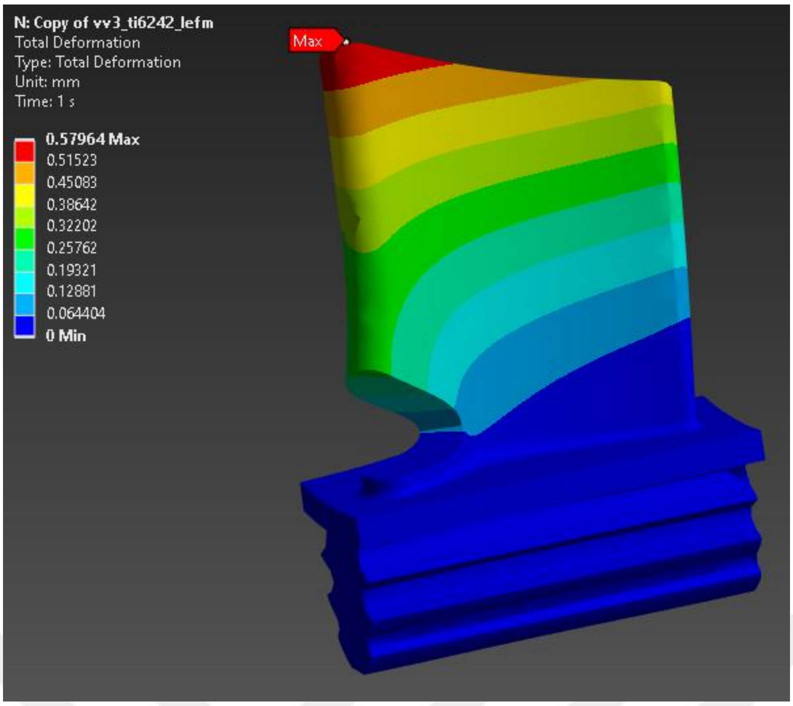

Figure 4.19 : Crack propagation of the turbine blade.

As similar to elastic structural analysis conducted in Section 3, the maximum deformation occurs on the tip of the blade as the value of 0.57964 mm. In addition, the total deformation through all analysis is plotted in the figure as shown in the figure. As it is expected, the total deformation on the blade tip increment is proportional to crack extension value.

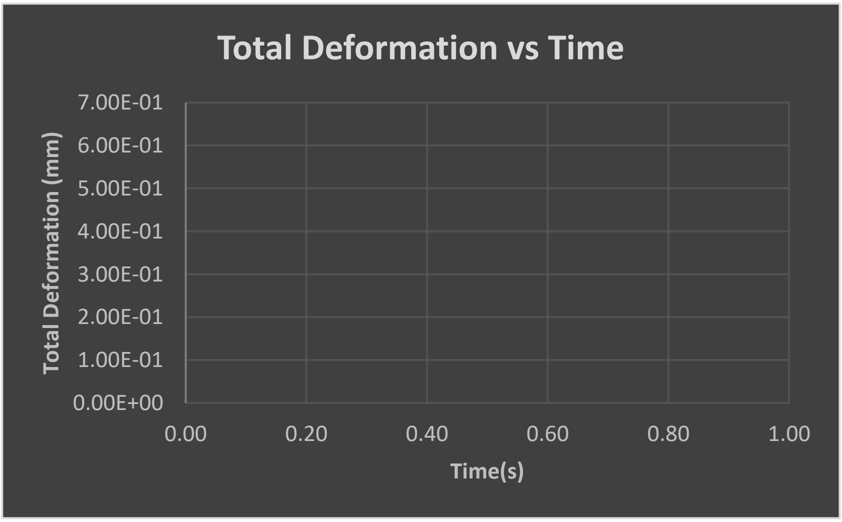

Figure 4.20 : Total deformation versus analysis time of the turbine blade analysis.

The maximum stress intensity factor of mode 1 (K_1) can be seen in the figure as 3321.6 MPa.mm^0.5 in the Contour 6 at the end of the analysis.

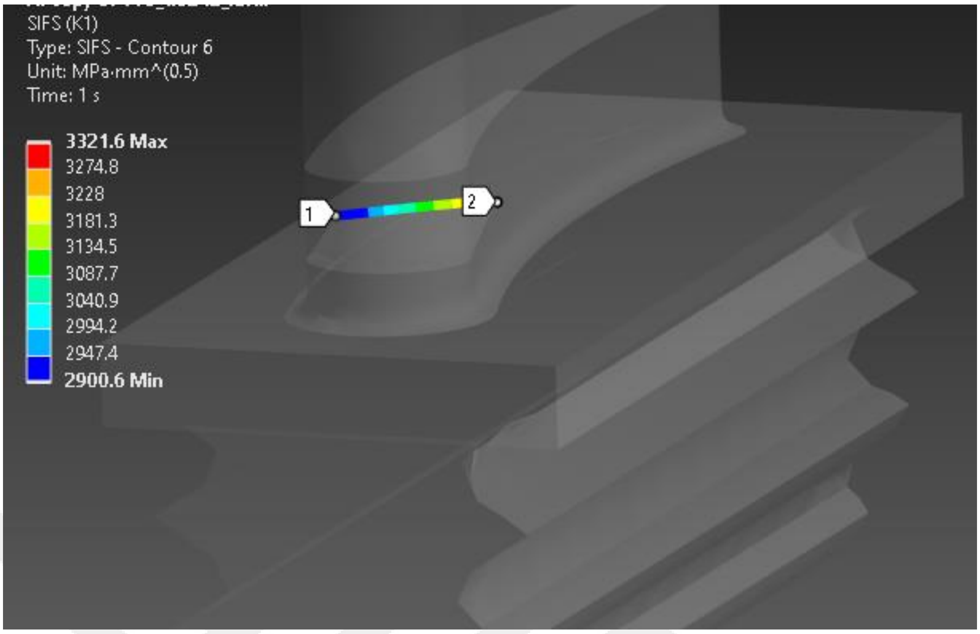

Figure 4.21 : The maximum stress intensity factor at the end of the analysis.

Stress Intensity Factor of Mode 1 (K_1) can be plotted according to contour results in the figure:

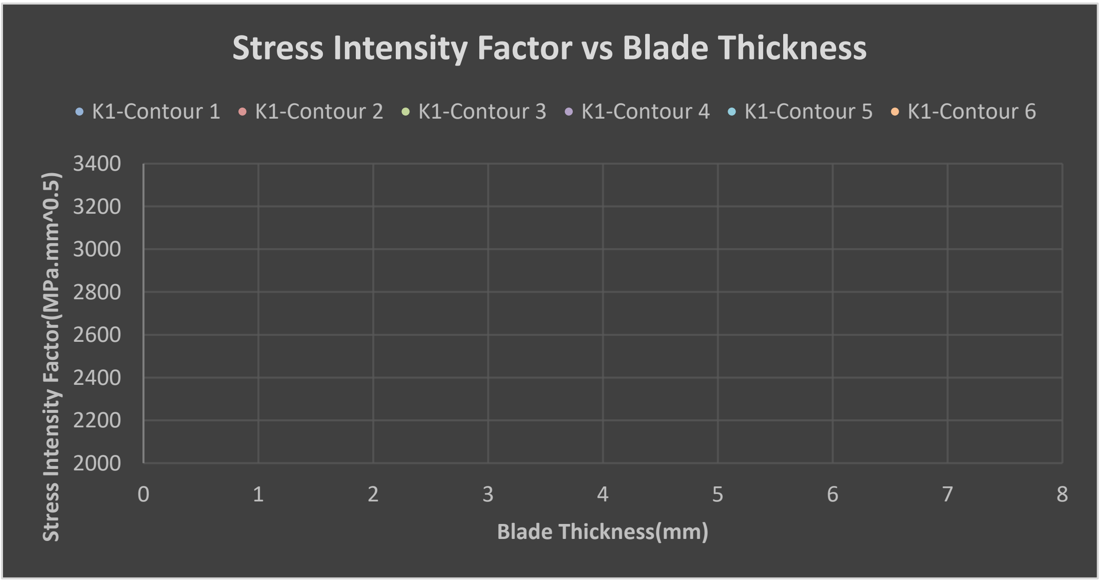

Figure 4.22 : Stress intensity factor contours.

As it is seen in the figure, all other five K1 Contours except Contour 1 curve are consistent within each other. This situation may occur due to singularity points created by coarse mesh on the crack surface.

4.3 The Results of the Machine Learning Model

After using the linear regression model, the predicted test data values of Stress Intensity Factor and the corresponding finite element solution results were calculated as shown in the figure below:

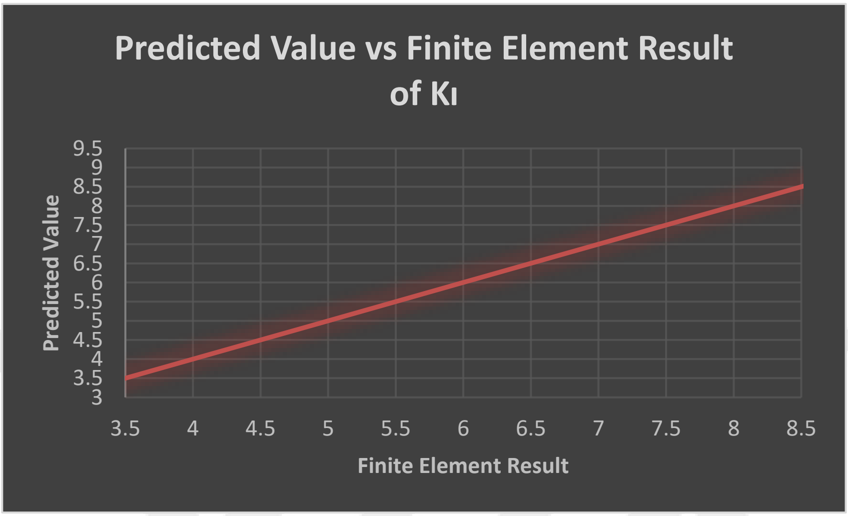

Figure 4.23 : Predicted values vs finite element results.

As it is seen in the figure, the predicted value of stress intensity factor is comparable with finite element calculated results. In this figure, the data points should be closer to the centerline represented by redline in order to have low error.

Moreover, the error percentage between finite element results and predicted values can be calculated by using the term residual.

In machine learning, residuals refer to the differences between the observed values and the values predicted by a model. The residual can be calculated as follows:

$$Residual = y_{predicted} - y_{actual} \tag{4.11}$$

By using this equation, residual curve of the prediction can be drawn as follows:

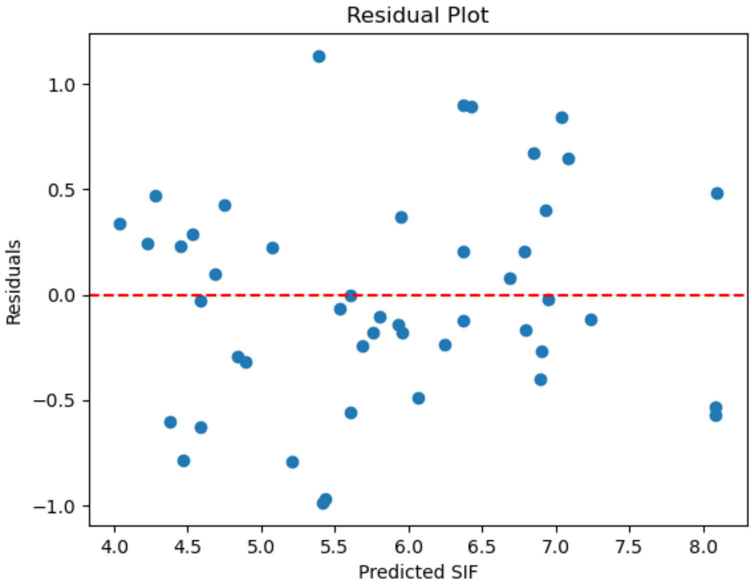

Figure 4.24 : Residual plot of the machine learning model.

The maximum residual was occurred as 1.13 where predicted value of the stress intensity factor is 5.38973 and the stress intensity from finite element analysis is 6.523549. This error may be decreased by adding more data to training set.

5. CONCLUSIONS AND RECOMMENDATIONS

In this thesis, the general parameters of both Linear Elastic Fracture Mechanics and Elasto Plastic Fracture Mechanics were investigated by completing three different studies. The main purpose of these studies was to investigate effects of the different geometric parameters and loading conditions on structures used in daily basis.

In the first two sections, a general concept and the required knowledge about different fracture mechanics approaches, as well as machine learning algorithms. Someone would use this knowledge to use in their future studies.

In the first study, a Compact Tension Test Specimen was studied in terms of both Linear Elastic Fracture Mechanics and Elasto-Plastic Fracture Mechanics. In this study, the test specimen was subjected in tensile loading from its pin holes. The study was conducted in two different approaches: the empirical calculation and the finite element method calculation. When the results of this study compared, it is seen that the empirical and numerical results are consistent within each other. Someone could use both empirical and numerical methods that stated in the relevant chapter in order to obtain proper results.

In the second study, a turbine blade which was under the centrifugal force as in the gas turbine engine was investigated in terms of Linear Elastic Fracture Mechanics. Firstly, a static structural analysis was conducted to determine stress critical regions as they are also important for crack growth. Moreover, a semi-elliptical crack on the leading edge near the stress critical region was assumed and its propagation was investigated by using ANSYS SMART Crack Growth module. At the end of the analysis, it is seen that crack was extended for 9.5408 mm. This type of failures has significant effect in the gas turbine engine environment since the blade-out situation may lead catastrophic event in the aviation.

Finally, a machine learning model was created by using data extracted by parametrizing geometric dimensions and loading conditions of the CTT in the first study. The database consists of 235 rows was exported from ANSYS Mechanical in order to use as training database in the machine learning code. In this code, linear regression algorithm from sklearn's library. The predicted stress intensity factors are comparable with the values extracted from finite element analysis in terms of errors.

It is clear to state that this thesis scope establishes a fundamental baseline to explore fracture mechanics further.

REFERENCES

[1] Murray, C. (2015, October 12). *Engineering disasters: SS Schenectady, a lesson in brittle fracture*. Design News. https://www.designnews.com/assembly/engineering-disasters-ss-schenectady-a-lesson-in-brittle-fracture, date retrieved 29.06.2024

[2] **Griffith, A. A.** (1920). The phenomena of rupture and flow in solids. Philosophical Transactions of the Royal Society of London. Series A, 221(582), 163-188.

[3] **Irwin, G. R**. (1957). Analysis of stresses and strains near the end of a crack transversing a plate. Journal of Applied Mechanics, 24(3), 361-364.

[4] **Rice, J. R.** (1978). Mechanics of ductile fracture - Criteria for void nucleation and growth. Acta Metallurgica, 36(11), 1565-1584.

[6] **Frangi, A., Novati**, **G.**(2003) BEM–FEM coupling for 3D fracture mechanics applications. *Computational Mechanics* **32**, 415–422 https://doi.org/10.1007/s00466-003-0510-8

[7] **Tran, V., Geniaut, S. (2012)** Development and industrial applications of X-FEM axisymmetric model for fracture mechanics. *Engineering Fracture Mechanics* **82**, 135-137

https://doi.org/10.1016/j.engfracmech.2011.12.002.

[8] **Mamandi, A., & Rajabi, M.** (**2016**). Fracture Mechanics Analysis and Fatigue Crack Growth Life Assessment for a Gas Turbine Blade Using FEM. *Journal of Mechanical Engineering, University of Tabriz*, *46*(2), 125-39.

[9] **Gupta, M. & Alderliesten, René & Benedictus, R.. (2014)**. A review of T-stress and its effects in Fracture Mechanics. Engineering Fracture Mechanics. 134. 10.1016/j.engfracmech.2014.10.013.

[10] **Budynas, R. G., & Nisbett, J. K. (2011).** *Shigley's mechanical engineering design* (Vol. 9, pp. 409-473). New York: McGraw-Hill.

[11] **Paris P.C. and Erdogan F.,** (1960), ‘’A critical analysis of crack propagation laws’’, Journal of Basic Engineering, (85), 528–534.

[12] **Saseendran, V. (2017).** *Fracture characterization and analysis of debonded sandwich composites*. Technical University of Denmark.

[13] **Chiesa, M. (2001).** Linking advanced fracture models to structural analysis.

[14] **Tada, H., Paris, P. C., & Irwin, G. R. (1985).** The stress analysis handbook. *Del Res Co*, B1.

[15] **ASTM International. (n.d.)**. Standard Test Method for Linear-Elastic Plane-Strain Fracture Toughness of Metallic Materials (ASTM Standard No. E0399-22). ASTM International. https://www.astm.org/e0399-22.html

[16] **Schulz, U., Leyens, C., Fritscher, K., Peters, M., Saruhan-Brings, B., Lavigne, O., ... & Caliez, M. (2003)**. Some recent trends in research and technology of advanced thermal barrier coatings. *Aerospace Science and technology*, *7*(1), 73-80.

[17] **Yahya, S. (2011).** *Turbines, compressors and fans* (Vol. 103, No. v4, pp. 0-035). Tata Mcgraw Hill Education Pvt. Ltd., New Delhi.

[18] **Davis, J. R.** (Ed.). (1995). *ASM specialty handbook: tool materials*. ASM international.

[19] **Abecassis, M., Köster, A., Esin, V. A., Chiaruttini, V., & Maurel, V. (2019)**. Crack growth behavior in dissimilar welded Ti based alloys under biaxial fatigue loading. *International Journal of Fatigue*, *118*, 209-224.

CURRICULUM VITAE

Name Surname : Görkem TÜREN

EDUCATION :

- **B.Sc.** : 2020, Istanbul Technical University, Faculty of Aeronautics and Astronautics, Astronautical Engineering

PROFESSIONAL EXPERIENCE AND REWARDS:

- 2021-Current, Whole Engine Structural Analysis Engineer- TEI-TUSAS Engine Industries, Eskişehir
- 2019-2020, Part Time Engineer- Turkish Airlines

PRESENTATIONS ON THE THESIS:

- **Türen, G & Türkmen, H. S.** 2024.Fracture Mechanics on Critical Rotor Component in Turbojet Engine. *5th International Mediterranean Congress*